

Oriental interaction and ordering of Cd_4 tetrahedra in a quasicrystal approximant

Woosong Choi* and Christopher L. Henley†

Laboratory of Atomic and Solid State Physics (LASSP), Clark Hall,
Cornell University, Ithaca, New York 14853-2501, USA

Marek Mihalkovič

Slovak Academy of Sciences

We model the quasicrystal-related structure $CaCd_6$, a bcc packing of icosahedral clusters containing tetrahedra which undergo orientational orderings at $T < 100$ K. We use general schemes to evaluate an effective Hamiltonian for inter-tetrahedron orientations, based on all-atom relaxations, either in terms of discrete cluster orientations, or of continuous rotation angles. The effective Hamiltonian is used in Monte Carlo simulations to find the (complex) ground state ordering pattern as a function of pressure. A preliminary investigation of thermal transitions found (in part of the pressure range) two different first-order transitions occurring below 100 K.

PACS numbers:

I. INTRODUCTION

Icosahedral i - $CaCd$ (and isostructural alloys such as i - $CdYb$) are the only known *binary* quasicrystals that have stable long-range-order.¹⁻³ Furthermore, their atomic structures represent a third family among quasicrystals, distinct from the previously known families of aluminum-transition metal and of Frank-Kasper packing (though including features of each). The structure contains large icosahedral “Tsai” clusters with *tetrahedra* of Cd atoms at their centers, which obviously breaks the cluster’s symmetry. It is built from icosahedral “Tsai” clusters consisting of several concentric shells; the outer shells have icosahedral symmetry, but the innermost one is a Cd_4 tetrahedron which can relatively easily rotate to different orientations. This obviously breaks the cluster’s symmetry.

This paper is concerned with the tetrahedra in $CaCd_6$, a bcc packing of the same Tsai clusters; an equivalent phase is stable in many other systems that form binary quasicrystals (e.g. $Cd-Y$, $Cd-Eu$, etc). Periodic structures having a unit cell like a fragment of a quasicrystal phase are called “approximants”; $CaCd_6$ is the simplest approximant of the i - $CaCd$ quasicrystal and others are known in nature.

Diffraction on $CaCd_6$ -type approximants has revealed various order/disorder transitions, which are ascribed to orientational ordering of the clusters. Thus, as a function of pressure (up to 5 GPa), Cd_6Yb has a complex phase diagram with six phases⁴. However, the exact orientations have not yet been determined experimentally or explained theoretically for any of these phases. In this paper, we compute a comprehensive set of interactions which, we hope, will predict the orientational ordering patterns and transition temperatures, and may serve as a starting point to address the role of orientations in stabilizing the quasicrystal phase.

The first modeling of tetrahedron energies in $CaCd_6$ ⁷ used ab-initio energies and started by *assuming* the experimentally refined sites¹³. Thus it was a sort of energy-guided fit, resolving the correlations in partially-occupied sites found from diffraction.

Later, Brommer *et al* performed a multiscale analysis to

understand the interaction and show the transition behavior: first building inter-atomic potentials,¹⁵ then modeling the nearest-neighbor interactions with 42 parameters (minus 6 constraints)¹⁶, and finally performing some Monte Carlo simulations with this effective cluster Hamiltonian¹⁶. Our paper should be considered a followup of this work.

In this paper, we build a systematic method find the effective interactions of tetrahedra (or similar inner clusters in other materials) from numerical relaxations. We give a natural way to eliminate arbitrary redundant freedoms in the interaction, so as to ensure the physical relevance of the fitted parameters in our model Hamiltonian, leading to a better view of the interactions (Section II D 3). A singular-value decomposition is used to identify the dominant contributions in the potential (and, in principle, to reduce the number of terms needed to represent it). We also show (Sec. IV) how to extend the same framework from a discrete set of orientations to the whole orientation space, and try to infer the functional form of the cluster orientation interaction Hamiltonian. Moreover, in Sec. V we use the effective Hamiltonian to find the lowest energy states in super cells not accessed by Brommer’s original calculations¹⁹. We explore other low energy structures that are found in larger super cell Monte Carlo relaxations.

II. FRAMEWORK AND METHODS

In this section, we introduce the general concepts and methods used in the rest of the paper, specifically the nature of the inter-cluster effective Hamiltonian (Sec. II A), the microscopic calculation of relaxed energies (Sec. II B), and our scheme for extracting and processing the effective Hamiltonian (Sec. II D). Most of them are not specific to Tsai clusters with tetrahedra, but would also work for other kinds of reorientable interior clusters inside icosahedral clusters, such as the pseudo-Mackay icosahedron in AlIr or AlPdMn materials⁶.

Before specializing to the clusters, we will review the constant structure that surrounds them. In $CaCd_6$, it consists of a bcc packing of icosahedral Tsai clusters, with lattice constant 15.7Å. Each Tsai cluster consists of the following concentric

shells:

- (1) Zn_4 tetrahedron, radius 1.9\AA ;
- (2) Zn_{20} dodecahedral cage, radius $\sim 4.2\text{\AA}$;
- (3) Ca_{12} icosahedron, radius 5.56\AA ;
- (4) Zn_{30} icosidodecahedron, radius $\sim 6.4\text{\AA}$.

These clusters touch along the 3-fold direction, while there are a few more Zn atoms between clusters around the 2-fold direction. (Alternately, these Zn atoms may be reckoned to belong to large triacontrahedra of Zn on both vertices and midedges, which overlap along the 3-fold inter-cluster linkage.)

A. Cluster effective Hamiltonian

In this material, the low-energy degrees of freedom are the tetrahedron cluster orientations, represented by rotation matrices $\{\underline{\Omega}_i\}$ relative to some reference orientation, where $i = 1 \dots N_{\text{cell}}$ as there is one cluster in each of the N_{cell} primitive cells. The positions of all other atoms are taken to relax, so as to accommodate the tetrahedra;¹² they may, indeed, have large displacements, but these are dependent on $\{\underline{\Omega}_i\}$.

We define an effective cluster Hamiltonian $\mathcal{H}(\{\underline{\Omega}_i\})$ as the minimum energy taken over all possible configurations constrained to have that combination of orientations, allowing relaxations of the surrounding atoms as well as distortions of the tetrahedra.³⁴ This effective Hamiltonian breaks up into one-, two-, and many-cluster terms:

$$\mathcal{H}(\underline{\Omega}) = \mathcal{H}_1 + \mathcal{H}_2 + \mathcal{H}_3 + \dots \quad (2.1)$$

We will assume that the many-body interactions are negligible. Of course, the terms have the full symmetry of the crystal structure (minus the tetrahedra): for example, the one-body term is the same for all clusters and is invariant under the point group $m\bar{3} (=T_h)$.

There is a useful analogy between the cluster degree of freedom and a (classical) spin, a unit vector that is specified by only two Euler angles, in contrast to the 3×3 rotation matrix $\underline{\Omega}$ which requires three Euler angles. The two-cluster interaction is analogous to dipolar or exchange spin interactions, while the single-body potential $U(\underline{\Omega})$ is analogous to the single-spin spin anisotropies due to crystal fields. An even closer analogy is to the interacting, rotatable CN dipoles in $\text{KBr}_{1-x}(\text{CN})_x$.²⁰

1. Single-cluster terms and optimal orientations

The single-body terms are

$$\mathcal{H}_1 = \sum_i U(\underline{\Omega}_i) \quad (2.2)$$

The single-cluster potential $U(\underline{\Omega})$ includes a large contribution with icosahedral symmetry, reflecting the strong steric interaction between the tetrahedron and the dodecahedral Cd_{20}

cage around it. Because those cage atoms sit practically at the hard-core radius, it is not surprising if $U(\underline{\Omega})$ has some sharp and irregular-looking dependences on orientation. The single-body term is expected to have a somewhat smaller contribution with cubic symmetry, indirectly due to the Tsai cluster's outer shell being distorted by its surroundings.

These tetrahedra get from one orientation to another by a quasi-rigid rotation: rigid in the sense that the topological identity of the tetrahedron is maintained throughout, but in fact both the tetrahedron and its Cd_{20} cage undergo strong distortions. (Indeed, sterically the tetrahedron cannot never change orientations unless there are cooperative motions of the caging atoms.) A previous study¹² addressed the barriers and dynamics of a single Zn_4 tetrahedron in the Zn_6Sc approximant (isostructural with CaCd_6). The present paper is concerned only with static properties.

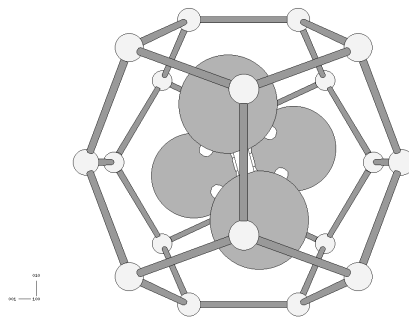


FIG. 1: Cd_4 tetrahedron in one of the twelve discrete optimal configurations. For visibility, the tetrahedron atoms are shown by large balls whereas those of the surrounding Cd_{20} cage are shown by small spheres. Bonds are drawn among the cage's atoms to highlight its dodecahedral shape. The orientation shown is $+X_r$, relative to the axes indicated.

Simulations¹⁶ found that tetrahedra in CaCd_6 tend to relax into one of twelve symmetry-related discrete orientations $\underline{\omega}_\mu$ (for $\mu = 1 \dots 12$), which must be minima of the single-cluster potential $U(\underline{\Omega})$. The fact that similar orientations are seen, regardless of how neighboring clusters are oriented, indicates the single-body term is at least as strong as the two-cluster term. However, certain discrete orientations are unstable in the presence of certain backgrounds of uniform surrounding orientations (see Sec. IID 1 below): so the single-body term is not *much* stronger than the cluster interaction.

A tetrahedron in one of the ideal orientations is shown in Figure 1. One of its twofold (actually $\bar{4}$) symmetry axes is lined up with one of the cubic coordinate axes; in the figure, this is the axis coming out of the paper. Now, there is no $\bar{4}$ symmetry in the icosahedron's point group (or more pertinently, one in the $2/m\bar{3}$ point group of the cluster center in cubic CaCd_6). Hence, the two ends of that twofold axis are inequivalent. (Indeed, Figure 1 shows the front two atoms are lined up under two atoms of the cage, whereas the two back atoms are rotated 90° .) Hence, there are six possible directions for that orientation axis which we label $\pm X$, $\pm Y$, $\pm Z$.

It is not quite stable for the two "front" tetrahedron atoms

to line up directly under the two nearby cage atoms. The cluster relaxes by rotating around the orientation axis by an angle of approximately $\pm 15^\circ$ – in either sense, thus spontaneously breaking a symmetry and giving twelve symmetry-equivalent directions. We indicate the rightwards (clockwise) or leftwards (counter-clockwise) rotation, *as viewed from the tetrahedron center*, by a subscript r or l , so our complete labels a form are written $+X_r$, etc. (Since orientations related by $r \leftrightarrow l$ are relatively close, we anticipate they may have similar interactions.)

In earlier experiments, Gómez and Lidin studied the x-ray diffraction of MCd_6 approximants, where $M = \text{Ca, Y, or rare-earth}$. They mapped out the continuous electron density inside Tsai clusters, which they were able to interpret in terms of a host of split positions representing tetrahedron orientational disorder, with preferred orientations of a single kind related by symmetry¹³. The apparent symmetry (see Ref. 18, Fig. 3) depended on the kind of large ion M , presumably reflecting the relative importance of the icosahedral and cubic components in the single-body term $U(\Omega)$ of the orientational Hamiltonian: icosahedral for $M = \text{Tm and Lu}$, cubic for $M = \text{Tb}$, and intermediate for $M = \text{Ho or Er}$. Their result for the case CaCd_6 agrees with the simulations of Ref. 16 as confirmed by our own: the tetrahedra sit in an asymmetric orientation.

2. Cluster pair terms

The two-body term is written

$$\mathcal{H}_2 = \sum_{i,j} V_{ij}(\Omega_i, \Omega_j). \quad (2.3)$$

The function V_{ij} is translationally invariant, depending on sites (i, j) only through the vector connecting them. It is expected to decay with separation. In this paper, the only separations included in the fit are the two kinds of nearest neighbors in the bcc lattice of cluster centers: the “ b ” linkage (separation vector equivalent to $[0, 0, 1]$) and the “ c ” type linkage (separation vector equivalent to $[1/2, 1/2, 1/2]$).

We now comment on the possible atomic-scale origins of the cluster effective interaction; however the results of this paper do not depend on understanding that, nor will they resolve it. A priori, one expects the cluster pair interaction has two kinds of contributions: mediated elastically, via displacements of intervening atoms, or mediated by the electron sea. The latter is expressed, within our framework, by the EAM or pair potentials (see Sec. II B 1, below) and more specifically by the long range Friedel oscillations characteristic of pair potentials in a metal. In contrast to the Al-TM and F-K classes of quasicrystal, Friedel oscillations do not appear to be crucial for the “Tsai cluster” class of quasicrystals¹⁵, which suggests the elastically mediated interaction should be dominant. Furthermore, if direct electronic interactions were dominant, one would expect the interaction of two clusters separated by a $[1, 0, 0]$ type bond to be invariant under a simultaneous rotation by 90° around the bond direction, which is not the case (see Sec. III). However, ab-initio calculations

by Ishii and collaborators found a substantial cluster interaction when atom positions are not relaxed, demonstrating that the direct electronic interactions are significant. Finally, we remark that in the isostructural compound ScZn_6 , the cluster-cluster interaction is much smaller¹².

Since the two-cluster term is mediated by a comparatively small distortion of the outer shells of the Tsai cluster, and/or is a sum of several potential terms, we anticipate that it is more smoothly behaved, and that the contributions from different neighbors will be additive.

B. Interatomic potentials

In order to do our fitting, we must build a database of relaxed energies coming from a lower, more exact level of description. We defined the cluster Hamiltonian as the relaxed minimum energy of the system, having fixed the orientation of every cluster. This opens up three questions:

- (1) How do we define or compute the energy of an arbitrary atomic configuration? (Sometimes these energies can be computed directly from ab-initio relaxations, but here we needed to use “classical” potentials.³⁵)
- (2) considering that the tetrahedra are typically distorted, what is our precise definition of cluster orientations? (This is required in order to define the family of configurations we are minimizing over.)
- (3) How do we implement this constrained minimization reliably?

This section explains our answers to each question including the important technicalities.

1. Potentials

Classical potentials are essential in various situations when molecular dynamics or relaxation is required in supercells containing many clusters. For the present problem, we used the minimum possible supercell which is $3 \times 3 \times 3$ or about 4000 atoms, which is too large for doing repetitive ab-initio relaxations.

Most of our calculations are based on the embedded-atom method (EAM) potentials fitted by Brommer and Gähler¹⁵. Their method of fitting is laborious and cannot be quickly repeated for a new material. As an alternative, we also tried the empirical oscillating pair (EOP) potentials¹⁷, which can be rapidly computed for any composition, but are valid only while the conduction electron concentration is held constant. Comparing results from the two potentials, as done in Sec III C below, may give a measure of the uncertainty of our conclusions, and/or a measure of the reliability of plain pair potentials in this system where their validity is less assured.

The (EOPP) pair potentials use an six-parameter analytic form which incorporates Friedel oscillations¹⁷. For this paper, they were fitted against a database of ab-initio results

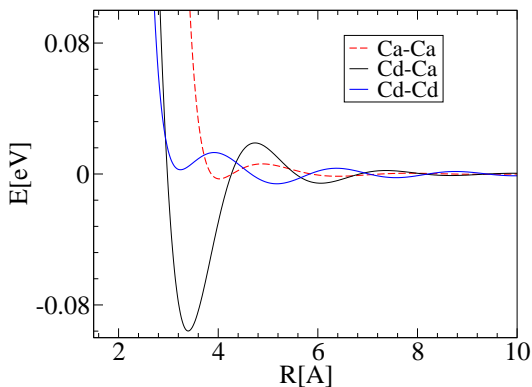


FIG. 2: Fitted “empirical oscillating pair potentials” (EOPP) for the Ca–Cd system.

with a total of 28 energy datapoints taken from relaxed $T = 0\text{K}$ structures, plus a single snapshot from a high-temperature molecular dynamics simulation at 1000K (of the cubic CaCd_6 structure) that gave over 7000 force datapoints. Our database of relaxed samples included all known Ca–Cd binary compounds (CaCd_2 in both CeCu_2 and MgZn_2 structures; Ca_3Cd_2 , Ca_2Cd_7 , and the B2 structure of CaCd ; and versions of the CaCd_6 approximant with six different ways of placing two Cd_4 tetrahedra in the cubic $1/1$ cell. Furthermore, we added structures that we took from similar systems, such as Ca_3Zn , Ca_2Cu , CaZn_3 , CaCd_{11} and finally the Frank-Kasper “Bergman” phase structure of AlMgZn . In the final iteration, the fit was biased so as to give forces as accurate as possible. The results are shown in Figure 2

It should be noted that the Tsai class of quasicrystals (and related alloys) is based on either Cd or Zn, both of which are known in their elemental forms to have an anomalous c/a ratio in the hcp lattice. Indeed, this might be related to the extremely non-rigid behavior of the Zn_{20} or Cd_{20} dodecahedral cages in the Tsai clusters, which is essential in allowing the inner tetrahedra to rotate at all. (See frames from the finite-temperature MD simulation of ScZn_6 , Figure 1 of Ref.¹²). We also know that pure Zn is one of the few cases in which the EOP potentials more or less fail¹⁷. Consequently, it is somewhat surprising that we find the EOP potentials succeed in CaCd_6 , in that the cluster Hamiltonian fit is similar to the result from EAM potentials (see Sec. III C).

C. Implementing cluster orientations and constrained relaxation

We need to establish an explicit practical mapping between atom positions and cluster orientations, the degrees of freedom at the two levels of description we want to relate. First we lay out the atoms-to-orientation mapping, and then its inverse, which actually means defining constraints for relaxation.

1. Defining cluster orientations

It is relatively easy to define the orientation $\underline{\Omega}$: the four inner atoms always *do* form some kind of tetrahedron, since it is sterically impossible for one of the atoms to pass through the plane formed by the other three.

Let \vec{r}_l be the position of tetrahedron atom l (for $l = 1, \dots, 4$), and define the center as $\vec{r}_c \equiv (\vec{r}_1 + \vec{r}_2 + \vec{r}_3 + \vec{r}_4)/4$; note that \vec{r}_c can deviate from the center of the surrounding cage. Also, define a regular reference tetrahedron by four unit vectors $\{\hat{t}_l\}$ in tetrahedral directions. (In the relaxation code, each tetrahedron’s initial prescribed orientation is used as the reference.)

Define a matrix \underline{M} with components

$$M_{\alpha\beta} \equiv \frac{3}{4} \sum_{l=1}^4 (\vec{r}_l - \vec{r}_c)_\alpha (\hat{t}_l)_\beta. \quad (2.4)$$

Now write the polar (=singular value) decomposition

$$\underline{M} = \underline{\Omega}_L \underline{M}_D \underline{\Omega}_R \quad (2.5)$$

where $\underline{\Omega}_L$ and $\underline{\Omega}_R$ are 3×3 rotation matrices, and \underline{M}_D is (positive) diagonal. It is easy to check that if $\{\vec{r}_i\}$ is a regular tetrahedron, then \underline{M}_D is a multiple of the identity and the actual tetrahedron is rotated, relative to the reference tetrahedron, by

$$\underline{\Omega} = \underline{\Omega}_L \underline{\Omega}_R \quad (2.6)$$

For a general tetrahedron, we take Eq. (2.6) as our *definition* of its orientation. It can be shown that (2.6) optimizes a measure of agreement, $\sum_{l=1}^4 (\vec{r}_l - \vec{r}_c) \cdot \underline{\Omega} \hat{t}_l$. If we had to do this for some other cluster with n_a atoms, we simply need a different set of ideal vectors and the above recipe still works, with the replacement $3/4 \rightarrow 3/n_a$ in (2.4).

There is an alternative way to think of orientation extraction, which is specific to the (present) case that the cluster has exactly four atoms, not in the same plane. We can uniquely and exactly represent the actual coordinates as

$$\vec{r}_l = \underline{M} \hat{t}_l + \vec{r}_c \quad (2.7)$$

since this is a set of $4(3)$ linear equations in $3^2 + 3$ unknowns (the components of \underline{M} and \vec{r}_c). In materials science, such a matrix defining an affine transformation of the atoms is called the *deformation matrix*. Indeed, for four atoms it gives the same result for \underline{M} as (2.4). As above, a polar decomposition (2.5) is performed to define $\underline{\Omega}$.

2. Constrained relaxation

In each constrained relaxation iteration, we assume a starting configuration in which each cluster already has its prescribed orientation, according to the definition based on polar decomposition. Conjugate gradient directions are constructed in the standard (unconstrained) fashion, but are then projected orthogonally into the allowed subspace, and one-dimensional minimizations are carried out along this projected direction.

We relax atom configurations, subject to the EAM or pair potentials, using a nonlinear conjugate gradient algorithm with Newton-Raphson and Fletcher-Reeves²³. Each successive conjugate-gradient iteration consists of a one-dimensional Newton-Raphson minimization (with up to 10 iterations) along the next conjugate-gradient direction. The stopping criterion is that the energy change per step is $\Delta E_{\text{step}} < 10^{-4}\text{eV}$. Typically, a few hundred conjugate-gradient iterations were needed.

The question is how to constrain all tetrahedron orientations $\{\underline{\Omega}_i\}$, while relaxing all atom coordinates. This amounts to $3N_{\text{cell}}$ nonlinear constraints, defined implicitly by (2.5) and (2.6). The basic approach is to linearize these constraints, defining a linear subspace within the manifold of all atomic coordinates.

Since the actual constraint is nonlinear, after some iterations the configuration would not exactly satisfy it. Therefore, every ~ 10 iterations we perform a nonlinear projection to reassert the orientation constraint. Namely, the actual relaxed positions $\{\vec{r}_i^r\}$ of the atoms in a tetrahedron are related to the ideal rotated positions $\{\underline{\Omega}\hat{t}_i\}$ by a deformation matrix \underline{M}' , then polar decomposed as $\underline{M}' = \underline{\Omega}_L \underline{M}_D \underline{\Omega}_R$ as in (2.5). We then replace $\underline{M}' \rightarrow \underline{M}_D$.

Specifically, let \underline{M}' be a possible additional infinitesimal deformation of the four atom positions $\{\vec{r}_i^r\}$ after a step, *relative to the previous positions* $\{\vec{r}_i^r\}$.

$$\vec{r}^r - \vec{r}_c = \underline{M}'(\vec{r} - \vec{r}_c), \quad (2.8)$$

with $\underline{M}' = \underline{I} + \underline{m}'$ with \underline{m}' small. Then the condition that \underline{M}' contains no rotation is that \underline{m}' is symmetric, which implicitly defines a set of linear conditions on $\vec{r}^r - \vec{r}_c$.

3. Comparison to unconstrained relaxation method

We want to contrast our constrained relaxation approach with the simpler alternative approach used in Ref. 16: plain *unconstrained* relaxation starting with prescribed initial orientations (preferably, optimal ones). One difference is that our constrained relaxation allows construction of a full Hamiltonian as a *continuous* function of orientations, as carried out below in Sectionsec:results-continuous, which allows simulating the orientation fluctuations found at $T > 0$ or mapping out the energy barriers for a cluster to reorient.

Using unconstrained relaxation, one accesses only the discrete set of orientations that are local minima. Usually, one implicitly depends on the assumption of a one-to-one correspondence between the combinations of initial orientations and final ones. In reality, it may happen – and did so in our study, in a few instances – that certain combinations of the discrete orientations in neighboring clusters are *not* locally stable: they relax into some other combination of orientations. A final, technical drawback to unconstrained relaxation is that even if that one-to-one correspondence exists, the actual ground state orientations deviate from the single-body optimum ones.

D. Extracting the cluster Hamiltonian

It is assumed we start by choosing a discrete list of representative possible orientations $\{\underline{\omega}_\alpha, \alpha = 1 \dots m\}$. In this work, these are either the twelve optimal orientations of the single-body terms (to obtain the discrete Hamiltonian in Sec. III) or else a finer-spaced grid that is meant to sample a continuous range of orientations (in Sec. IV). Except where noted, our set of orientations $\{\underline{\omega}_\alpha\}$ always has the full point symmetry of cluster site.

A dataset is then constructed of the relaxed energies $E_{\alpha\beta}$ for orientation $\underline{\omega}_\alpha$ in cluster site i and $\underline{\omega}_\beta$ in cluster site j , for all combinations of the two, while the other (“background”) clusters are held fixed. In CaCd₆, we consider (mainly) two kinds of pairs, which are the nearest-neighbor sites of the bcc lattice: those separated by $\langle 100 \rangle$ vectors and by $\langle 1/21/21/2 \rangle$ vectors. (We sometimes call these, respectively, “ b ” and “ c ” linkages, based on their role in the canonical-cell tiling²⁴.)

Our aim in fitting is to convert the array $E_{\alpha\beta}$ to an energy function in the form of the cluster Hamiltonian (2.1), with well-defined and compact formulas for the single-body term $U(\Omega)$ and pair term $V_{ij}(\Omega, \Omega')$.

1. Uniform background approach to isolate pairs

In order to properly fit the pair interaction of two clusters, they must be put in a sufficiently large supercell that they have only one significant interaction with each other (no interactions with an image of the neighbor through periodic boundary conditions in a different direction). When the cluster pair is related by the b type vector $[0,0,1]$, that demands a supercell of at least $3 \times 3 \times 4$ basic cells (i.e. 72 clusters).

It is not feasible to exhaustively enumerate all possible combinations of cluster orientations in the supercell and relax every configuration; our fits must be based on a subset of orientations. We will describe two different ways to choose this subset: exhaustive enumeration of a pair in a fixed background, which we used in this project, or random configurations of the whole system, used by Brommer *et al*¹⁶.

Each supercell configuration is specified by three orientations: $\underline{\Omega}_i, \underline{\Omega}_j$, the orientations of the two clusters whose interaction we want, and the background orientation $\underline{\Omega}_{bg}$, which is taken by all other clusters. While keeping $\underline{\Omega}_{bg}$ fixed, we enumerate all m^2 possible combinations of $(\underline{\Omega}_i, \underline{\Omega}_j)$ and (as described shortly below) extract a fit $V_{\alpha\beta}$. Thus, we get m independent fits, one for each background. (Due to symmetries not all of them are independent.) This provides some useful checks.

When our sampled orientations $\{\underline{\Omega}_\alpha\}$ are just the twelve optimal ones, which are symmetry equivalent, $U(\underline{\Omega}_\alpha)$ has the same value for every one so the correct result should be $U_\alpha = 0$. However, the presence of a particular background breaks the symmetry; in our fit, the pair interactions between cluster i or j and “background” clusters all get absorbed into U_α term, so it will be non-constant. But if we average U_α over all possible backgrounds, the symmetry should be restored. After we complete the fit for $V_{\alpha\beta}$, we can predict the apparent

single-body term due to the background, and check if this is consistent with the apparent single-body terms that were actually fitted. (Any disagreement suggests the importance of further-neighbor interactions with the background.)

In any case, provided we only have pair cluster interactions, we should still obtain an identical fit for $V_{\alpha\beta}$ regardless of the background. But actually, multi-body interactions including both of the selected clusters, and one or more of the background clusters, many contribute to the fitted $V_{\alpha\beta}$. Thus, any dependence of $V_{\alpha\beta}$ on the background signals the presence of multi-body interactions.

The uniform-background procedure relies on being able to generate any specified combination of orientations. This might fail, if we use unconstrained relaxation, because certain combinations of orientations might be unstable and turn in a different direction. In particular, we found that the background orientation $\underline{\Omega}_{bg}$ is $+X_r$, a varied cluster with orientation $-X_r$ very often is unstable, reorienting to $-X_l$. This problem is fixed by using a relaxation constrained to a particular orientation (see Sec. II C 2, above). Alternatively, it may be evaded by using the random-whole-system approach instead.

The random-whole-system approach was used by Brommer *et al*¹⁶ for CaCd₆. (It was also used²⁵ in Ir₂₃Al₄, a quasicrystal approximant from the Al-transition metal class, which has a different kind of orientable inner shell consisting of Al₁₀Ir in the pseudo-Mackay icosahedron cluster.) Produce 10^3 – 10^4 realizations of a supercell with a random combination of orientations and relax each one; if orientations are unstable, it is necessary to analyze the final state to ascertain the actual index α for each cluster. In each configuration, we find the count $N_{\alpha\beta}^l$ of cluster linkages of type l having the clusters in orientations $\underline{\Omega}_\alpha$ and $\underline{\Omega}_\beta$, respectively. Then we use a linear least-squares fit to express the total energy as

$$E_{rmtot} = \sum_{l,\alpha,\beta} E_{\alpha\beta}^l N_{\alpha\beta}^l. \quad (2.9)$$

Of course, symmetries are normally used so as to reduce the number of parameters.

We mention briefly a third way to construct a database, related in spirit to the uniform-background. (It is analogous to determining spin-spin interactions in a magnetic material by diluting it with nonmagnetic ions that are chemically equivalent to the magnetic ones, so that only isolated pairs of the latter occur.) We choose two clusters to vary through all combinations of interactions, but take a background having *no* orientational interactions, by replacing every other tetrahedron by a single large atom that takes up the same space; as it happens, the Ca atom is close to the right size. There is no averaging over backgrounds since there is only one kind.

The single-atom replacement trick was successfully applied to the isostructural compound ScZn₆, but only to study the effects of the single-cluster term on the dynamics (the inter-cluster interactions are, in any case, weak in that material). We experimented with this method for pair interactions in CaCd₆, but these preliminary investigations suggested that the systematic errors are too large for us to trust the results quantitatively.

2. Symmetry properties of the discrete interaction matrix

Consider the permutation symmetries of the interaction matrix \underline{V} that follow from the space-group symmetry operations of the CaCd₆ framework, which affect \underline{V} in two ways. First, the rotation part of these operations permutes orientations within the set $\{\underline{\Omega}_\alpha\}$ (except in the trivial case of pure translations). Second, there are three interesting cases for the action on the cluster centers: both may map to themselves, they may be swapped, or one maps to itself and the other maps to a different cluster. For each of these cases, it will be convenient to write $E_{\alpha\beta}$ and $V_{\alpha\beta}$ using matrix notation as arrays \underline{E} and \underline{V} , which in general are *not* symmetric. The action of a point group operation g on cluster orientations is written with an $m \times m$ permutation matrix, \underline{P}_g . (Here we mean the matrix in which each row and column contains exactly one element 1, and the others are zero, so multiplication by this matrix induces a permutation of the indices.)

First, for a lattice symmetry operation that keeps both clusters fixed, invariance of the energy under this symmetry is represented by

$$\underline{P}_g \underline{V} (\underline{P}_g)^T = \underline{V}. \quad (2.10)$$

This requires that the bond vector is invariant when g acts at the midpoint.

Second, consider a rotational symmetry h that exchanges the two clusters. (In practice we need only consider inversion; all others are products of inversion and a symmetry of the first kind.) Now we get

$$\underline{P}_h \underline{V} (\underline{P}_h)^T = \underline{V}^T. \quad (2.11)$$

Thirdly, consider a rotation g that, acting on site i and maps $i \rightarrow i$ but sends $j \rightarrow k$. We get

$$\underline{P}_g \underline{V} (\underline{P}_g)^T = \underline{V}' \quad (2.12)$$

The use of (2.12) is that, having computed the interaction matrix for a pair separated by (say) $[0, 0, 1]$, we find the interaction matrix for symmetry related bond vectors such as $[100]$.

3. Redundant parameters: pair interaction resolution

Whenever one fits an effective Hamiltonian to configurations of discrete variables, one finds linear dependencies between the counts of certain local patterns and certain other ones. (Here “local pattern” means a particular combination of two or more discrete variables in nearby sites.) Thus, if every local pattern is allotted an independent coupling coefficient, the values of these coefficients will be ill-determined: a whole family of parameter sets gives identical energies for all possible configurations. Such dependencies arise when the discrete variables are Ising spins²⁶ or tiles (“decorated” by atoms) in quasicrystal-related phases²⁷; they arose in the previous fit of a cluster Hamiltonian¹⁶ and were handled by arbitrarily setting certain coefficients to zero.

In fact, interacting clusters are the simplest of the cases where these dependencies are observed. Our task is to write

$$E_{\alpha\beta} = E_0 + U_\alpha + U'_\beta + V_{\alpha\beta}. \quad (2.13)$$

The difficulty is that the solutions of (2.13) are ill-defined, since it is invariant under

$$V_{\alpha\beta} \rightarrow V_{\alpha\beta} - A_\alpha - A'_\beta; \quad (2.14a)$$

$$U_\alpha \rightarrow U_\alpha + A_\alpha; \quad (2.14b)$$

$$U'_\beta \rightarrow U'_\beta + A'_\beta, \quad (2.14c)$$

where $\{A_\alpha\}$ is an arbitrary set of energy shifts. Within an extended crystal, with bonds oriented in several directions, there will be different functions A_α and A'_α associated with each direction of bond; the one-body term gets shifted by the sum of all these. Thus, even if we constrained all $U_\alpha \equiv 0$, that would not resolve the indeterminacy in $\{V_{\alpha\beta}\}$. There is a similar indeterminacy in the single-cluster term:

$$U_\alpha \rightarrow U_\alpha - B; \quad (2.15a)$$

$$U'_\beta \rightarrow U'_\beta - B'; \quad (2.15b)$$

$$E_0 \rightarrow E_0 + B + B'. \quad (2.15c)$$

We do resolve it by imposing the simple rule

$$\sum_\alpha V_{\alpha\beta} = \sum_\beta V_{\alpha\beta} \equiv 0; \quad (2.16a)$$

$$\sum_\alpha U_\alpha \equiv \sum_\beta U'_\beta \equiv 0. \quad (2.16b)$$

Given an initial set $E_{\alpha\beta}$, it is easy to implement Eq. (2.16a) using Eqs. (2.14) with

$$A_\alpha \equiv \frac{1}{m} \left(\sum_\beta E_{\alpha\beta} \right); \quad (2.17a)$$

$$A'_\beta \equiv \frac{1}{m} \left(\sum_\alpha E_{\alpha\beta} \right). \quad (2.17b)$$

After that we enforce Eq. (2.16b) by applying (2.15) with $B \equiv (\sum_\alpha U_\alpha)/m$ and similarly B' .

E. Singular Value Decomposition methods

The matrix of interactions $V_{\alpha\beta}$ for the discrete orientations has m^2 entries and this implies a large number of fit parameters, even after symmetries are taken into account and redundancies eliminated. For example, Ref. 16 – taking the discrete approach – fitted a separate interaction parameter for every inequivalent combination of orientations of the nearest or second-nearest cluster neighbors, which amounted to 42 interactions (slightly fewer after removing redundancies).

However, we anticipate that some combinations of these parameters are unimportant. Imagine, e.g., if a cluster developed a charge q_α dependent on its orientation, then the cluster orientation would be a Coulomb interaction proportional to $q_\alpha q_\beta / |R_{ij}|$ and thus of completely separable form.

To parametrize such an interaction for m orientations, we do not need $O(m^2)$ numbers, but only one overall strength and a list of $O(m)$ charge strengths q_α . An electric dipole interaction is similar, but since the dipole moment has three components, the interaction would take the form

Our recipe to reduce parameters is to posit that the interaction matrices can be put in the form

$$V_{\alpha\beta} = \sum_{\mu=1}^{m'} \sigma_\mu g_\alpha^\mu g_\beta^{\prime\mu}. \quad (2.18)$$

The implicit idea here is that the clusters are weakly perturbing some “field” which fills the space between them. Think of g_α^μ as the “charge” presented by the first cluster when it is in orientation α , similarly $g_\beta^{\prime\mu}$ as the “charge” presented by the second cluster, while σ_μ is the effective interaction of these charges (expected to decay with separation). More exactly, μ indexes different kinds of “charge”, or different components of the same charge. For example, if the tetrahedron atoms carried a literal charge, then μ would index the cluster’s moments (monopole, dipole, etc) and their tensor components (three for the dipole case). In CaCd₆, we expect the interaction is mediated by elastic strains of the intervening atoms, or possibly by direct couplings (which are represented by the oscillating tail in the pair potentials shown in Figure 2, or analogous tails in the EAM potentials¹⁵).

For definiteness, let’s augment (2.18), by an orthonormal condition $\sum_\alpha g_{\mu\alpha} g_{\nu\beta} = \delta_{\mu\nu}$. Then, these two equations are equivalent to the *singular value decomposition*, or in matrix notation

$$\underline{V} = \underline{g}^T \underline{\sigma} \underline{g}' \quad (2.19)$$

where $\underline{\sigma}$ is the diagonal matrix \underline{g} and \underline{g}' are orthogonal matrices of singular values (which we take to be nonnegative and decreasing). In this form, we have $m' = m^{36}$. But our expectation (to be checked!) is that the singular values σ_μ rapidly get smaller, so we can truncate (2.18) after (say) three terms and reduce the 42 parameters to a handful.

In practice this decomposition is much more powerful when symmetries come into play. Following the analogies to (electric or elastic) dipoles and quadrupoles, we imagine that the dependence of the “charge” on orientation Ω could be written as a smooth function $g(\Omega)$ with the angular dependence of an orientational harmonic. This idea is tested in Section IV

III. RESULTS: DISCRETE ORIENTATIONS

In this section, we use the framework of Section II to fit a cluster potential for the twelve discrete, symmetry-related optimal orientations, similar to the form used in Ref. 16. Our microscopic Hamiltonian is defined by EAM potentials of Ref. 15. For each relaxation, we use an initial structure in which the “regular” atoms (all atoms excluding the tetrahedra) are in their averaged positions with cubic crystal symmetry (space group $Im\bar{3}$), as refined in Ref. 13 (this structure has

	$+X_r$	$-X_r$	$+X_l$	$-X_l$
$+X_r$	-2.8	0.5	4.2	-0.4
$+Y_r$	-8.6	5.7	-1.9	3.9
$+Z_r$	-5.2	2.0	-1.1	3.9
$-X_r$	-6.8	3.9	-7.3	4.2
$-Y_r$	6.0	-6.3	3.2	-1.1
$-Z_r$	0.3	2.6	3.2	-1.9
$+X_l$	-5.3	3.5	3.9	0.5
$+Y_l$	-2.3	11.7	2.6	2.0
$+Z_l$	-17.6	11.7	-6.3	5.7
$-X_l$	9.6	-5.3	-6.8	-2.8
$-Y_l$	21.3	-17.6	0.3	-5.2
$-Z_l$	21.3	-12.3	6.0	-8.6

TABLE I: Interaction matrix for two clusters separated by $[1/2, 1/2, 1/2]$ ($=c$ -linkage), using EAM potentials (in meV). Due to the threefold symmetry of this linkage, all interactions are invariant under cyclic permutations (xyz) in the labels when applied to both clusters; thus columns are given here only for the “ X ” orientations.

the Pearson symbol cI208). Each tetrahedron is initially regular (having radius 1.775\AA and centered on the Tsai cluster center) and in the prescribed orientation $\underline{\Omega}_i$.

A. Cluster pair interaction

We computed interactions for two kinds of cluster pairs, separated by the vector $[1/2, 1/2, 1/2]$ ($=c$ linkage) or $[0, 0, 1]$ ($=b$ linkage), placed in a $3 \times 3 \times 3$ supercell. We used the uniform background method and averaged over the twelve possible backgrounds; as required by symmetry, the averaged single-body term was zero (i.e. all orientations were equivalent). The resulting pair interactions are given in Tables I and II.

To make sense of the computed interactions, it is essential to consider the local symmetry of the cluster pair, which is reflected in the symmetry of $V_{\alpha\beta}$ as laid out in Sec. II D 2.

For the c pair, the point group (centered on the linkage’s midpoint) $\bar{3}$ (D_3); the subgroup which maps each cluster to itself is 3 (C_3). This threefold rotation, in terms of our orientation labels, just cyclically permutes (XYZ) without changing the \pm or r/l part of the labels. As for the b pair of clusters, its point group is $2/m\bar{m}$ (D_{2h}) and the subgroup that maps each cluster to itself is $2m$ (C_{2v}) which has order 4. Its generators are the mirror operations m_x and m_y , which respectively invert the x or the y coordinates. (Remember we singled out the z direction by aligning the pair with it.) The action of m_x , for example, is to switch $+X \leftrightarrow -X$, not switch the sign of the Y or Z orientations, and in all cases to switch $r \leftrightarrow l$. Finally, in all cases it is convenient to let inversion be the fundamental operation that swaps the two clusters; its action on our labels is to always switch $+ \leftrightarrow -$ and always switch $r \leftrightarrow l$. (Note that any proper rotation always preserves the r/l indices whereas any improper rotation always switches them.) We take advantage of these symmetries to reduce the number of columns displayed in the interaction matrices.

	$+X_r$	$-X_l$	$+Y_r$	$-Y_l$	$+Z_r$	$-Z_l$
$+X_r$	17.4	-17.0	6.7	6.5	-1.1	0.8
$+X_l$	18.7	-16.5	6.5	6.7	-0.6	0.4
$-X_l$	-17.0	17.4	-7.0	-8.5	-0.6	0.4
$-X_r$	-16.5	18.7	-8.5	-7.0	-1.1	0.8
$+Y_r$	-8.5	6.5	-2.5	-2.3	0.6	-0.7
$+Y_l$	6.5	-8.5	4.4	2.8	1.4	-1.4
$-Y_r$	7.0	6.7	-2.3	-2.5	1.4	-1.4
$-Y_l$	6.7	-7.0	2.8	4.4	0.6	-0.7
$+Z_r$	0.4	0.8	-1.4	-0.7	-3.8	4.1
$+Z_l$	0.	0.4	-0.7	-1.4	-2.6	4.0
$-Z_l$	-0.6	-1.1	1.4	0.6	2.6	-3.8
$-Z_r$	-1.1	-0.6	0.6	1.4	3.0	-2.6

TABLE II: Interaction matrix $V_{\alpha\beta}$ for two clusters related by $[0, 0, 1]$ vector ($=b$ -linkage), in meV. In all interaction matrices the cluster 1 orientation is given in column headings, and cluster 2 orientation by row headings. The interaction is invariant if one switches $r \leftrightarrow l$ in both labels, so the columns with “ $+l$ ” and “ $-r$ ” labels are omitted.

1. Justification of functional form

Can we make sense of the patterns of interactions? First of all, we see that just a few combinations have much larger interactions than any others. In the c -linkage case, for example, the pair $(-Z_l, +X_r)$ and permutations has interaction 21.3 meV; due to inversion symmetry relating the two clusters [we are using (2.11)], this has the same interaction as the pair $(-X_l, +Z_r)$. In turn that is equivalent by cyclic permutation to $(-Y_l, +X_r)$ in our table, which is indeed 21.3 meV. The interaction $(-Y_l, -X_r)$ is almost as big, -17.6 ; this is equivalent to The interaction $(+X_l, +Y_r)$, i.e. $(+Z_l, +X_r)$ in the table, by inversion. Overall, it can be seen that the r orientations have stronger interactions than the l orientations.

Similarly, in the b interactions (Table II), we that X orientations (of all flavors) have by far the largest interactions, while Z orientations have the least.

If the clusters were far apart and weakly perturbing their surroundings, we would expect the inversion of a cluster would have exactly the opposite coupling, in the case of a tetrahedron, since it moves the atoms to the places complementary to them. To say this another way, consider the union of a tetrahedron and its inverse, i.e. a cube: whatever is the lowest nonzero “multipole moment” of the tetrahedron, we would expect that one to be zero in the case of the cube. Thus, we expect that *approximately* $V_{\alpha\beta} = -V_{\alpha'\beta}$ when α and β are related by inversion. This expectation is borne out in the b -bond interactions, as can be seen by comparing adjacent entries in columns 1 and 2, 3 and 4, or 5 and 6. However, in the case of the c -linkage it does not work well: the largest interactions ($(-17.6$ and $+21.3)$ are related (see the leftmost column) by $+Z_l \leftrightarrow -Z_l$.

A somewhat surprising fact is that the size of c -bond interactions is the same as that of the b -bond interactions; this is confirmed (see below) by the fact the respective dominant singular values from each interaction are practically the same. The best absolute measures, the matrix norms, are respectively 94.7 and 83.1, for a ratio ~ 1.1 . One would have expected the c -bond interaction to be larger – by a factor of

σ (meV)	irrep	$+X_r$	$-X_l$	$+X_l$	$-X_r$
81.51	A	-0.1380	-0.0054	-0.3181	0.4616
33.79	E	0.2339	0.4564	0.4140	0.4819
		-11.7°	164.9°	-66.9°	138.0°
5.443	A	0.4204	0.0739	-0.3675	-0.1268
2.278	E	0.7060	0.1414	0.2760	0.2684
		177.1°	-68.0°	-109.8°	161.6°
1.385	E	0.2987	0.2812	0.5896	0.3883
		142.7°	176.5°	-68.5°	-79.5°
1.330	A	-0.2329	0.4944	-0.1170	-0.1445
3.288×10^{-2}	E	0.1557	0.5994	0.2673	0.4600
		33.4°	65.8°	55.8°	-56.0°

TABLE III: Singular values and right singular vectors for c -linkage. This cluster pair has a symmetry under cyclic permutations (XYZ) and consequently every singular vector falls into one of the two representations of that symmetry group. Those labeled I follow the identity representation; the omitted columns for Y and Z type orientations have the same amplitudes as the corresponding (shown) columns for X type orientations. The representations labeled 2 are twofold degenerate, and take the form $A \cos \phi_X$, $A \cos(\phi_X + 120^\circ)$, and $A \cos(\phi_X + 240^\circ)$ for the X , Y , and Z entries, where (A, ϕ_X) is shown in the table; a second, degenerate singular vector takes the same form but with 90° added to all the phases.

~ 1.5 , if the interaction simply scaled as $1/R^3$.

2. Singular Value Decomposition

Applying the singular value decomposition analysis to the data in Tables II and I. yields the results in Tables IV and III. Again, these need to be understood in light of the point symmetries. In particular, every singular vector must transform under one of the irreducible group representations, which have been identified and indicated in the tables. The irreps of 3 are named A (trivial) and E (two-dimensional); the irreps of $2/m$ are named A_1 (trivial), A_2 , B_1 , and B_2 .

Having identified the largest entries in the interaction matrix, we can interpret the leading singular values and their singular vectors. For example, let's approximate the b -linkage interaction matrix by keeping only its largest terms, found in the 4×4 subblock represented by the upper left eight entries in Table II). They are all close to ± 17 meV, with a pattern of signs that gives a rank-1 matrix. There would be just one nonzero singular value $\sigma = 4(17)\text{meV} = 68$ meV. Its singular vector would have four entries $\pm 1/2$, for the four kinds of X orientation, and zero on all others. The pattern of signs is $(+ - + -)$ in the convention of Table IV, which corresponds to the B_2 representation; in this approximation the top row of the table would read $(-0.5, 0, 0, 0)$ and we see this is a good approximation of the actual singular vector. Similarly, the second singular vector in Table IV is approximately $(0, 0, 0.5, -0.5)$, expressing the difference between $Z+$ and $-Z$ orientations.

It can also be noted that, for the b interaction, both of the two leading singular vectors treat the r and l variants orientations the same; if we retained only these two terms, that truncated interaction sees only six kinds of orientation, with the r and l variants lumped together. On the other hand, the leading

σ (meV)	irrep	$+X_r$	$+Y_r$	$+Z_r$	$-Z_l$
81.45	A_2	0.4621	-0.1908	0	0
15.59	A_1	0.1282	-0.1625	0.4881	-0.4196
3.836	B_1	0.2402	0.3507	0.2705	-0.2557
3.212	B_2	0.3727	0.3333	0	0
2.745	A_1	0.3780	-0.2321	-0.3247	0.0329
1.375	B_1	0.0484	0.0077	0.4245	0.5612
2.733×10^{-1}	A_1	-0.0858	-0.2940	0.2701	0.4894
2.073×10^{-1}	B_1	0.3552	-0.3313	0.1046	-0.1312
1.364×10^{-1}	B_2	-0.3333	0.3727	0	0
1.307×10^{-1}	A_2	0.1908	0.4622	0	0
2.017×10^{-2}	B_1	-0.2526	-0.1308	0.4854	-0.3200
	irrep	signs X	signs Y	signs $+Z_{r/l}$	signs $-Z_{l/r}$
	A_1	+++	+++	++	++
	B_1	+-+	+-+	+-	-+
	A_2	++-	+-+	00	00
	B_2	+-+	+-+	00	00

TABLE IV: Singular values σ and right singular vectors for b -linkage. The singular vectors belong to representations of the point group $2m (=C_{2v})$, as given in the second column: Each singular vector has twelve entries, one for each of the orientations (column labels). The four orientations beginning with direction “ X ” or “ Y ”, e.g. “ $(+X_r, +X_l, -X_l, -X_r)$ ”, always have the same amplitudes apart from sign, so only the first column is printed from each group of four. Similarly, in each of the pairs “ $(+Z_r, -Z_r)$ ” and the and “ $+Z_l, -Z_l$ ” only one of the two is needed. The pattern of relative signs for the group of four or the pair depends on the group representation, as given at the bottom of the table.

singular vector for the c interaction is very far from treating r and l equivalently.

B. Testing validity of discrete effective Hamiltonian

1. Checks from the fitting process

We have checked the validity of the orientation potentials in multiple ways. First, we report the results of two checks which are inherent to the uniform-background scheme for fitting, as explained in Sec. IID 1.

The first check is that, in the fit with a particular background, the apparent one-body energy vector entirely represents interactions with the background orientation, and therefore has a low symmetry. The apparent one-body energy varies between $+0.03\text{eV}$ and -0.05eV for most backgrounds.

Next, from the fitted pair interactions of our chosen clusters, we can predict the summed pair interactions of either cluster with its 13 $[100]$ and $[1/2, 1/2, 1/2]$ neighbors in the fixed background, for each of the fixed backgrounds. The agreement is excellent: the root-mean-square residual is 2.6 meV when the varied clusters are a $[1/2, 1/2, 1/2]$ pair, or 2.3 eV when they are a $[100]$ pair. This residual is due to either multi-body interactions or to more distant neighbor interactions (with the background clusters).

Incidentally, in a preliminary study, we directly tested the assumption that farther neighbor interactions are significantly weaker, by directly fitting $V_{\alpha\beta}$ trial fits of the pair interaction

and therefore could be omitted. For second nearest-neighbors displaced by the vectors $[0, 1, 1]$ and also $\frac{1}{2}[1, 1, 3]$. (This was only carried out using a neutral background of Ca-filled clusters, as mentioned in section IID 1.) These interaction matrices gave singular values more than an order of magnitude smaller than those of the nearest-neighbor interactions.

The second check from fitting is that, insofar as multi-cluster interactions can be neglected, different backgrounds should give an *exactly* identical interaction matrix – even if there are longer range pair interactions. We found that this is largely so. To quantify the dependence on background we considered how a particular element $V_{\alpha\beta}$ of the 12×12 interaction matrix varies while we cycle $\underline{\Omega}_{bg}$ through all 12 possible values, and compute the standard deviation of $V_{\alpha\beta}$.

In the case of the $[1/2, 1/2, 1/2]$ cluster linkage, the average standard deviation is about 1–2 meV. The larger interactions and larger standard deviations were between any tetrahedron of orientation $+X/Y/Z_r$ and any one of orientation $-X/Y/Z_t$.

In the case of the $[1, 0, 0]$ linkage, the standard deviation was typically ~ 0.6 meV, i.e. half as big as for the c -linkage. Deviation was larger than average for the 4^2 interaction terms that combine $X-X$ type orientations by a factor of almost two, and smaller by a factor of nearly two in the 8^2 terms not involving any X type orientation. (The $X-X$ pairs had by far the strongest interactions, too),

To summarize, the multi-cluster interactions, as measured by the standard deviation of $V_{\alpha\beta}$ while the background is varied, is $\sim 15\%$ of the cluster pair interaction, for both kinds of linkage. Thus, the multi-cluster interactions are significant, but an order of magnitude down from the dominant pair interactions.

2. Tests by direct comparison with total energies

To fully validate the effective Hamiltonian fitted from uniform backgrounds (in $3 \times 3 \times 3$ supercells), we should test it on databases with and the energies computed with configurations other than the fitting database. Our test datasets was a $3 \times 3 \times 3$ supercell with in which randomly oriented tetrahedra were placed, and then relaxed in two ways (see Sec. IIC 2), giving two variant datasets:

- (1) relaxed with the continuous orientation $\underline{\Omega}_i$ held strictly fixed;
- (2) the same random orientations, unconstrained relaxation so the orientation can change

(In the latter case, it was assumed without checking that every cluster's orientation remains in the discrete well belonging to optimal orientation with which it was initialized.)

Figure 3 shows scatter plots comparing the effective Hamiltonian prediction (vertical axis) with the actual EAM interaction, for the two random datasets and also the input fitting dataset. An offset of about $+94.30$ eV/cluster has been subtracted, representing the EAM energy of all the atoms in one primitive cell.³⁷ A systematic constant offset is visible due to

the use of constrained relaxation. It should be noted that this is entirely canceled out in way we fit the pair interactions (see Sec. IID 3).

The scatter of the total energy appears to be a bit under ± 0.1 eV, coming from $2 \times 3^3 = 54$ clusters, or a total of $54 \times 14/2 = 378$ linkages, since each has $(8+6)$ c - and b -type neighbors. If we imagine that each interaction deviates randomly and independently from the fitted energy, this random energy comes to ~ 4 meV/linkage, consistent in magnitude with the residuals estimated just above (in Sec. IIIB 1).

The fitted Hamiltonian can be further checked for transferability to a larger super cell. Figure 4 shows a comparison between the actual atomic energies of a random configuration in a $4 \times 4 \times 4$ with the predictions from the fitted cluster-pair Hamiltonian. It too shows very high correlation between the energies which suggests that the effective Hamiltonian is doing a decent job of capturing the essence of the interactions.

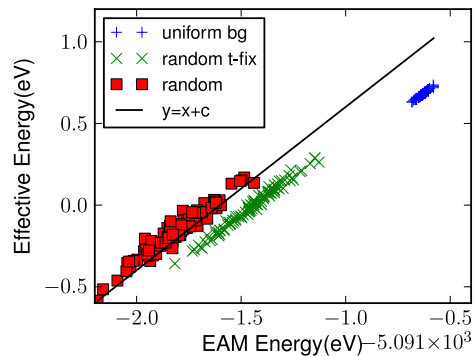


FIG. 3: Scatter plot, showing effective Hamiltonian prediction compared to the relaxed energies, for a $3 \times 3 \times 3$ superlattice with each cluster in a random discrete orientation (out of the twelve optimal ones). Different symbols refer to different conditions of the fit: $+$ = the uniform background configurations (constrained relaxation) used for the fit; \times = random configurations relaxed with the constraints (Sec. IIC 2) and \square = relaxed unconstrained. These last are offset to the left, due to the energy reduction when tetrahedra (under forces from neighboring tetrahedra) relax to orientations slightly different from the discrete minima of the single-tetrahedron orientational potential.

C. Cluster Hamiltonian with pair potentials

All the fits mentioned till now were derived from EAM potentials. In this section, we have redone them using fitted (EOPP) pair potentials. It is not *a priori* obvious whether pair potentials should be adequate for our problem. The Cd_{20} cage atoms make large displacements in response to rotations of the tetrahedron, which might have the same cause as the anomalous c/a ratio in hcp elemental cadmium, which (at least is the similar element Zn) is poorly captured by the EOPP potentials¹⁷. The response of cage atoms must be the most important determinant of the tetrahedron's elastic interaction with

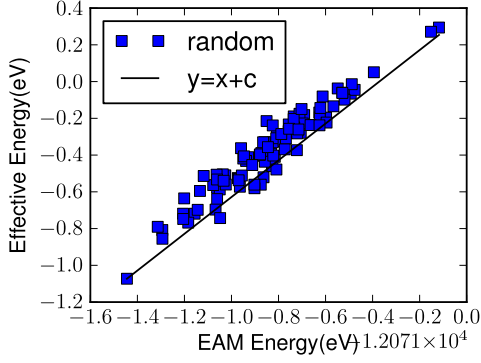


FIG. 4: Scatter plot, comparing energies of relaxed atomic configurations in $4 \times 4 \times 4$ supercells to those predicted by the discrete cluster Hamiltonian, which was fitted from a smaller ($3 \times 3 \times 3$) supercell.

	$+X_r$	$-X_r$	$+X_l$	$-X_l$
$+X_r$	-0.0055	0.0008	0.0013	0.0051
$+Y_r$	-0.0069	0.0012	-0.0020	0.0025
$+Z_r$	-0.0021	-0.0012	0.0044	0.0025
$-X_r$	-0.0054	0.0030	-0.0024	0.0013
$-Y_r$	0.0027	-0.0031	0.0017	0.0044
$-Z_r$	-0.0027	0.0008	0.0017	-0.0020
$+X_l$	-0.0072	0.0063	0.0030	0.0008
$+Y_l$	-0.0137	0.0144	0.0008	-0.0012
$+Z_l$	-0.0158	0.0144	-0.0031	0.0012
$-X_l$	0.0126	-0.0072	-0.0054	-0.0055
$-Y_l$	0.0220	-0.0158	-0.0027	-0.0021
$-Z_l$	0.0220	-0.0137	0.0027	-0.0069

TABLE V: Interaction matrix for two clusters separated by $[1/2, 1/2, 1/2]$ ($=c$ -linkage), using pair potentials (in meV), using the same conventions as Table I.

its surroundings.

The result is that the interactions derived from pair potentials are remarkably consistent with those from EAM. A sample of this is given by the singular value decomposition of the c -bond interaction (Table VI), in which the top three singular vectors show great agreement.

σ	irrep	$+X_r$	$-X_l$	$+X_l$	$-X_r$
89.95	A	-0.1054	-0.0094	-0.3398	0.4546
23.83	E	0.2102	0.3825	0.4328	0.5374
		-150.8°	107.9°	-26.9°	141.9°
18.43	A	0.4158	0.0999	-0.3514	-0.1643
5.612	E	0.6982	0.3914	0.0286	0.1588
		178.0°	70.2°	160.5°	146.9°
2.706	E	0.2354	0.4099	0.6458	0.1615
		-62.1°	24.2°	-6.7°	30.3°
2.221	A	-0.2569	0.4898	-0.1050	-0.1279
3.075×10^{-2}	E	0.2822	0.4462	0.2478	0.5714
		-163.5°	-121.0°	55.1°	48.3°

TABLE VI: Pair-potential results: singular values and right singular vectors for c -linkage, in same format as table III

σ (meV)	irrep	$+X_r$	$+Y_r$	$+Z_r$	$-Z_l$
58.15	A_2	0.4469	-0.2241	0	0
Z 8.421	A_1	0.1003	-0.1868	0.5309	-0.3581
3.699	B_2	-0.2619	0.4259	0	0
3.487	B_1	0.0172	-0.1127	0.2854	0.6266
2.369	A_1	-0.3560	0.0052	0.3651	0.3364
2.098	B_1	0.3177	0.2864	0.3579	-0.0774
1.051	A_1	-0.1728	0.3630	0.0383	0.4187
8.957×10^{-1}	A_2	0.2241	0.4469	0	0
2.749×10^{-1}	B_1	0.3844	-0.2561	-0.2704	0.0100
1.925×10^{-1}	B_1	-0.0314	-0.2995	0.4662	-0.3183
6.157×10^{-2}	B_2	0.4259	0.2619	0	0

TABLE VII: Singular values σ and right singular vectors for b -linkage, as derived from pair potentials, using the same conventions as Table IV

This gives some reassurance as to the independence of our results from the specific potentials used. It may help justify the adoption of fitted pair potentials for related compositions (in particular ScAn_6) for which EAM potentials are not available, subject to the caution that the EOPP potentials must be re-fitted if the lattice is compressed or expanded.

IV. RESULTS: CONTINUOUS ORIENTATIONS

Till now, the discussion in this article was limited to a set of discrete reference orientations, which are determined by the local minima of the one-cluster potential. In fact, that is not a necessary condition for our analysis: our method of relaxation with the rotation constraint (Section II C 2) lets us evaluate the the effective Hamiltonian for *any* set of orientations, whether stable or not.

To proceed, we define some discrete set $\{\omega_\alpha\}$ of m orientations that samples the continuous space. We adopt the uniform background set-up (Sec. IID 1, letting two interacting clusters run through all combinations of $(\omega_\alpha, \omega_\beta)$ while keeping the other clusters in fixed orientations. Once again, we use the singular-value decomposition (SVD) (2.18) as the fitting procedure to obtain the single-cluster and pair terms $U(\underline{\Omega})$ and $V(\underline{\Omega}, \underline{\Omega}')$. Since there are now thousands of distinct pair combinations, the SVD becomes a necessity in the case of continuous orientations, rather than an option as it was with the discrete version of the interaction.

The continuous formulation offers multiple opportunities. First, we can now map out the single-cluster term, separated from the interaction term. This opens up the possibility of detecting metastable, higher energy minima, of finding the barriers between discrete wells. and of simulating temperatures so high that large deviations from the optimal orientations are typical in the ensemble.

Secondly, we obtain the cluster pair interaction valid for any combination of continuously variable orientations. even when the interaction term is so strong as to destabilize the local well for certain combinations of orientations (or strong enough to significantly displace the orientations from the reference orientation). Finally, going past the SVD this naturally pushes us to a further step of simplification in representing the coupling

of each cluster, namely orientational harmonics, and these offer the possibility to unify the basis of functions $g(\Omega)$ used in representing all the different interactions of a cluster.

In this section, we start off by laying out the quaternion-based mathematical framework needed to describe rotations (Sec IV B). Then we carry out two forms of continuous fit. First (Sec. IV A), we limit the rotations of both tetrahedra to a single rotation axis. Second (Sec. IV C) we endeavor to sample *all* rotations. In either analysis, we do find that just the first two or three σ_μ values matter, and the singular vectors can be interpolated by smooth functions, thus vindicating the motivation of the singular value analysis of the potentials.

A. “One-dimensional” rotations

The simplest continuous sub-space of the manifold of orientations consists of all rotations around one axis, parametrized by a single Euler angle. We choose this axis such that the rotations connect (at least) two of the known optimal orientations. Specifically, we choose a zero orientation of $+X_r$ so that rotation around the x -axis passes through $+X_r$ to $+X_l$, $-X_r$, and $-X_l$. (a rotation by exactly π takes $+X_r$ to $-X_r$ or $+X_l$ to $-X_l$.) Rotations around y and z axis are also used; we will call the respective rotation angles Λ_x , Λ_y , and Λ_z . The sampling points are spaced by 5° along each of the three circles. These three data sets are combined into a single one, which we call the “three-circle” point set, with a total of $36+72+72=180$ sample points (the Λ_x rotation runs only to 180° since it repeats after that.)

The first result of the fit (before any SVD analysis) is the single-body potential, a byproduct of the processing mandated in Sec. IID 3. (Recall that such information cannot be obtained from the discrete analysis of Sec. III.) The results are shown in Figure 5(a).

Each deep well is one of the optimal directions. Angle $\Lambda_{x,y,z} = 0$ is, by definition, the orientation $+X_r$. Rotating around the x axis, we encounter $-X_l$ at 90° ; also, at $\Lambda_x \approx 30^\circ$ and $\Lambda - x \approx 120^\circ$, we meet $+X_l$ and $-X_r$, respectively. At either $\Lambda_y = 180^\circ$ or $\Lambda_z = 180^\circ$, we meet $-X_r$; at $\Lambda_y = \pm 90^\circ$ we meet $\pm Z_r$, while at $\Lambda_z = \pm 90^\circ$ we meet $\pm Y_r$. The double well at $\Lambda_x = 105^\circ \pm 15^\circ$ is responsible for the $\pm 15^\circ$ rotation of the tetrahedra in optimal states (of these, the well at $\Lambda_x = 90^\circ$ actually appears to be destabilized by the uniform background.)

In principle, the single-body output has contributions (as in the discrete case) from the pair interactions of the background, as well as from the true single-cluster term $U(\underline{\Omega})$; however the latter contribution is much larger. The background contribution merely creates slight energy offsets, visible in the figure, between wells which ought to be symmetry-equivalent: e.g. along the Λ_x circle, $-X_r$ appears to be lower in energy than $+X_r$, by ~ 0.04 eV. (We would eliminate the background contribution if we averaged over all possible backgrounds, as was done in the discrete analysis of Sec. III, but that was not carried out in our treatment of the continuous rotations.)

Next comes the singular vector analysis, with the singular vectors normalized according to Eq. (4.3). The resulting

Singular value	c-linkage			b-linkage		
	C3	P600	R30	C3	P600	R30
σ_1	80.28	86.04	68.06	95.20	76.52	67.86
σ_2	51.64	50.87	43.04	16.17	25.80	18.40
σ_3	28.70	48.25	31.93	11.00	6.648	6.416

TABLE VIII: First three singular values from three continuous data sets (in meV). Here “C3” is the three-circle data set (Sec. IV A), while “P600” and “R30” are the polytope 600 and the random 30 data sets (Sec. IV C).

singular values are included in Table VIII. The overall magnitudes are comparable to the discrete result, and some differences can be explained away because the three-circle data set is not even approximately uniform: e.g., as it starts from $+X_r$, it over-represents the four X flavors of discrete orientation. (Since those ones have the strongest pair interactions, according to Table II, it is not surprising that the dominant singular value for the b -linkage for the C3 data set (Table VIII) comes out 20% larger than the corresponding singular value for optimal orientations in Table IV.) Note also that the third singular value is not so well separated here from the second one, as was the case with the discrete orientations (Sec. III A 2).

In conclusion, the three-circle data set gave a decent indication of how smoothly the potential varies between the relevant discrete orientations, and it goes along with a convenient way of plotting singular vectors along cuts in this three-dimensional parameter space. However, it completely fails when we try to transfer to orientations that are not near to those three circles in orientation space. Thus, this approach does not suffice to provide a parameterized representation of the complete functional form for *all* possible orientations, as we would need to use this in a simulation with continuous angles.

B. Mathematical handling of continuous rotations

The most uniform way to parametrize rotations in three dimensions is by four-component unit *quaternions*: for a rotation of angle θ about axis $\hat{\theta}$, the first component is $\cos(\theta/2)$ and the other three are $\sin(\theta/2)\hat{\theta}$. Thus the quaternions map out a hypersphere, which corresponds 2-to-1 with rotations (since antipodal quaternions represent the same rotation). The quaternion components are related to the three Euler angles as follows:

$$q_0 = \cos \alpha \quad (4.1a)$$

$$q_1 = \sin \alpha \sin \theta \cos \phi \quad (4.1b)$$

$$q_2 = \sin \alpha \sin \theta \sin \phi \quad (4.1c)$$

$$q_3 = \sin \alpha \cos \theta \quad (4.1d)$$

Here 2α is the total rotation angle, and (q_1, q_2, q_3) equals $\sin \alpha$ times the unit vector of the rotation axis.

The proper measure in rotation space is uniform on the unit hypersphere parametrized by (4.1). Thus, the normalization

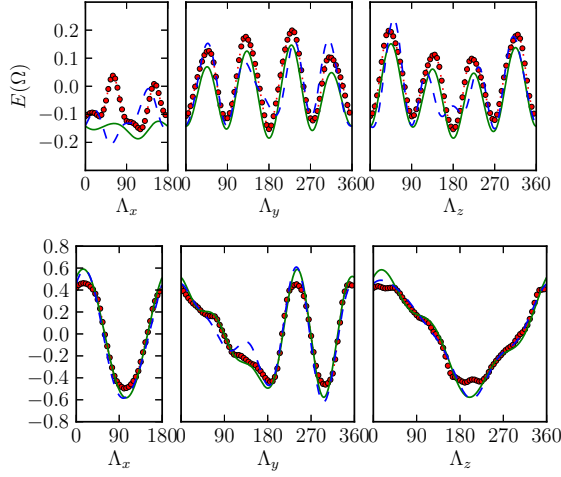


FIG. 5: Fitted potentials for a cluster pair separated by $[0, 0, 1]$, displayed along three circular paths in rotation space parameterized by rotation angle Λ , Λ_y , Λ_x respectively. (a). single-body potential term $U(\Lambda_k)$ along the three circles (the Λ_x plot has period 180°). (b). Singular vector $g(\underline{\Omega})$ for the dominant singular value. (The singular vector for the second cluster is related by symmetry to that of the first.) Different lines indicate the following databases: (i) Dots [red online] = actual measured energies, sampled every 5° for a total of 180 points; this was the database for the “three-circle” fit; the smooth interpolated version of that, using hyperspherical harmonics, closely follows the data and is not shown. (ii) solid line [green online] = hyperspherical harmonic fits using Polytope 600. (300 orientations placed on the vertices of the regular polytope 600 in rotation space, fitted by SVD, and then interpolated using hyperspherical harmonics). A random fit “R150” was practically identical to “P600”. (iii) The dashed line [blue online] is “R30”, a database of 30 randomly chosen orientations, symmetrized according to the two mirror planes of the $[0,0,1]$ cluster linkage that do not swap clusters, for a total database of 120 points.

convention used for functions of rotation space is

$$\int d^3\omega \equiv \left(\int_0^{2\pi} \sin^2 \alpha d\alpha \right) \left(\int_0^\pi \sin \theta d\theta \right) \left(\int_0^\pi d\phi \right). \quad (4.2)$$

In particular, the total volume of ω -space is $(2\pi)^2$. Hence, we normalize a discrete singular vector (g_1, g_2, \dots) by

$$\sum_{k=1}^m |g_k|^2 \equiv \frac{m}{\pi^2}. \quad (4.3)$$

If our singular vector is the sampling of a normalized continuous mode $u(\omega)$ and if the sampling points are uniformly distributed, this will be equivalent to the normalization of the continuous mode. With such a normalization, singular values obtained from different constructions ought to have similar magnitudes, as is borne out in Table VIII.

1. Hyperspherical harmonics

We assume the interaction (or singular vector) is a smooth function in rotation space. The standard way to parametrize

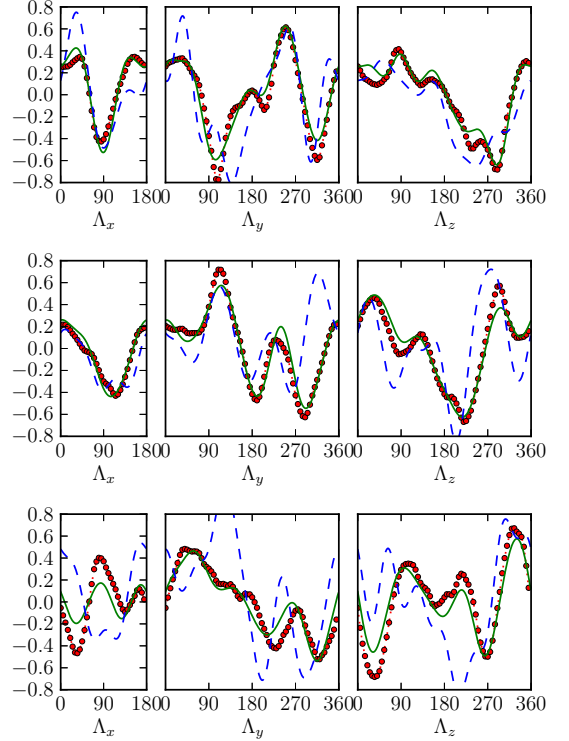


FIG. 6: Same as Figure 5(b), but for clusters related by a “c” type separation. Two additional singular vectors are illustrated, as they are comparable in strength to the leading ones. Note that this fit is less successful, and in places the R30 fit fails. (a) Dominant singular vector (b) Second singular vector (c) Third singular vector. (The single-body energy plot is very similar to Figure 5(a) and is not shown here.)

such a function with a small number of fitting parameters, is a series expansion using some basis of orthogonal functions, ideally tailored to the symmetry of the space. When our data, sampled at necessarily sparse points in rotation space, is expressed in this basis, it can be thought of as simply an elaborate kind of interpolation.

The natural basis for the 3-sphere is the *hyperspherical harmonics*, analogous to expanding in spherical harmonics on a 2-sphere. (These are also commonly used in the theory of textures in materials science²⁸.) We adopt the definitions and normalizations for real hyperspherical functions from Eq. (6) of Ref. 28. These carry three indices: N , the total “hyperangular momentum”, with L and M to label different functions within the same representation. The real hyperspherical harmonics, in terms of the three Euler angles α, θ, ϕ , are then given by

$$Z_{NL}^{MC}(\omega) = z_{NLM} C_{N-L}^{L+1}(\cos \alpha) P_L^M(\cos \theta) \cos M\phi, \quad (4.4a)$$

$$Z_{NL}^{MS}(\omega) = z_{NLM} C_{N-L}^{L+1}(\cos \alpha) P_L^M(\cos \theta) \sin M\phi, \quad (4.4b)$$

where $C_{N-L}^{L+1}(\cos \alpha)$ is a Gegenbauer polynomial and $P_L^M(\cos \theta)$ is an associated Legendre function. These are orthonormalized with respect to the measure of Eq. (4.2), and

the normalization constant is

$$z_{NLM} = (-1)^{L+M} \frac{2^L L!}{\pi} \left[(2L+1) \frac{(L-M)! (N+1)(N-L)!}{(L+M)! (N+L+1)!} \right]^{1/2}. \quad (4.5)$$

C. Fits from sampling all orientations

It is necessary to devise some roughly uniform way to sample rotation space. We have tried two ways. First, we choose m quaternions uniformly spaced by placing them on one of the regular polytopes of icosahedral symmetry, the higher-dimensional analog of an icosahedron. However, it appears the polytope is inefficient because it has too much symmetry, and some places in rotation space are far from any point of the polytope. Our second approach is to select a random list of orientations $\{\omega_k\}$ and then apply the mm symmetries around the $[0, 0, 1]$ bond, i.e. those which preserve the two cluster positions. This turned out to work much better.

Applying the SVD yields one dominant singular value, along with a corresponding dominant singular vector $g_{\mu\alpha}$ as shown in Figure 5 (b,c). This represents the leading mode of the two-body interaction, and looks like sampling a largely sinusoidal function of ω_α [Figure 5(b)]. The y -axis shows a noticeably non-sinusoidal profile;

Fitting the coefficients of hyperspherical harmonic expansion to the most important singular vector yields, for the case of the $[0, 0, 1]$ (or “ b ”) interaction, coefficients in the $N = 6$ and $N = 8$ hyperspherical harmonics. Further harmonics were not needed and (when included) seemed to reflect sampling arbitrariness and not improve the fit. For the $[1/2, 1/2, 1/2]$ (i.e. “ c ”) interaction, we additionally needed $N = 12$ in order to get a decent fit.

On the other hand, the hyperspherical fits of the $[1/2, 1/2, 1/2]$ (“ c ”) cluster pairs require $N = 12$ hyperspherical harmonics in addition to the $N = 6$ and $N = 8$ used for the b -interactions, and still this is not so good a fit. Furthermore, the second and third largest singular values are non-negligible in the case of the c interaction, as shown in the figure. We conjecture that the c interaction is the most complicated simply because it is the shortest.

Figure 5(c) shows how the fitted singular vectors compare against the singular vector from slices measurements. The fits from polytope-600 and the three-circle data set both give reasonable approximations of the actual data. In contrast, polytope-120 (not shown) fails completely, which can be readily understood from the fact that the orientations in polytope-120 are too spaced too far apart (72° from each other), and furthermore the cuts shown in the figures do not even have to go through the sampled orientations.

V. ORIENTATIONAL ORDERINGS

A great advantage of the fitted Hamiltonian approach is that one may discover the optimal structures for systems that were not included in the fitting database (and which could not have been included, because they are too big). In this spirit, we take the discrete effective Hamiltonian from Section III and find what is predicted for the ordering pattern at low temperatures. We used Monte Carlo annealing in supercells to discover the ground state.

Watanuki et al.⁴ discovered pressure-induced phase transitions in the CdYb₆ cubic crystal. Therefore, we extend our studies to nonzero pressure, so as to make contact with experiments that show different ordered states appearing in a range of pressures < 10 GPa.

A. Strain, pressure, and bulk modulus

To extend our calculations to varying hydrostatic pressure, we reran calculations of the energies and ground states constrained to various strain values, separated by 0.002 (or by 0.010 for strains greater than 0.01). The corresponding pressure P (at $T = 0$) was then evaluated by recalculating the energy at slightly different cell volumes V and using $P \approx (\Delta E)/(\Delta V)$. The pressure/strain relationship suggests that changes in the lattice constant at the $T = 0$ transitions are quite small.

Note that the “strain 0” results, reported in previous sections, used a cell constrained to an a priori lattice constant. The present calculation shows that (with the EAM potentials we are using) they do not exactly not correspond to zero pressure, in fact we found zero pressure at negative strain. A possible physical meaning to study even more negative strains (with negative pressures) is as follows. In isostructural compounds with the large atom species varied, an increase (decrease) in its effective radius is appears as a negative (positive) “chemical pressure”, so that we might see a similar phase diagram except for a shift along the P axis.

The bulk modulus grows rather uniformly with pressure: from about 80 GPa to 300 GPa over the range from our most negative pressure (strain -0.020) to the largest one (strain $+0.040$). Specifically it was around 150 GPa at $P = 0$ or 200 GPa at $P \approx 1$ GP. We do not know of any experimental measurement of the bulk modulus of CaCd₆; measurements of the (similar) quasicrystal phase i -CdCa gave a bulk modulus 68.1 GPa at zero pressure²⁹.

We also estimated the pressure using all possible $2 \times 2 \times 1$ supercells with a pair of clusters of all possible orientation combinations, placed in uniform backgrounds of all possible orientations. This was the same database used to construct the cluster pair potentials. These are higher-energy structures, so this is roughly like an ensemble of infinite temperature (so far as cluster orientations are concerned). We found that (i) the pressure was higher by ~ 1.5 GPa, (ii) at zero pressure, the strain was -0.008 , i.e. an increase of the lattice constant which could be interpreted as an orientational contribution to the thermal expansion. (iii) the bulk modulus is $\sim 20\%$ higher

in the ZY structures found at small negative strain, to $\sim 10\%$ higher around the transition to the ZY structure around strain 0.07, and roughly unchanged at the highest pressures.

B. Monte Carlo search for ground state in supercells

We performed Monte Carlo (MC) simulations using the fitted discrete cluster Hamiltonian in a $4 \times 4 \times 4$ supercell, i.e. 128 clusters. (Sizes over ~ 50 clusters cannot be equilibrated with plain Monte Carlo owing to the frustrated interactions.) The lowest energy configuration encountered during a run was saved and defines the ground state ordering.

1. Results: ordered states

The predicted ground state orientation pattern does change under pressure. We have found at least three distinct optimal states as P is varied. The transitions between them at $T = 0$ are necessarily first-order: since every tetrahedron falls into one of twelve discrete orientations, there is no way that one pattern can evolve continuously into a distinct one.

The three $T = 0$ phases are shown in Figures 7 and 8.

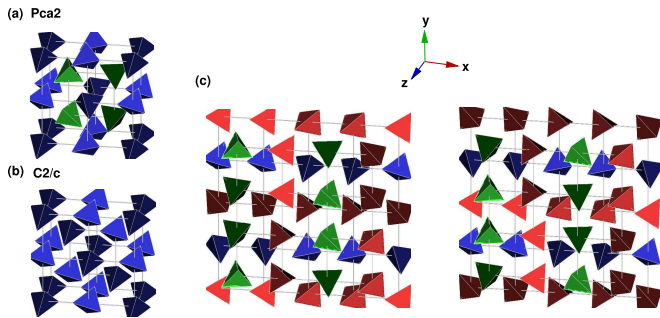


FIG. 7: [Color online] Phases of tetrahedron order in CaCd_6 found from simulation at various pressures. [Online: tetrahedra aligned with X , Y or Z directions are colored red, green, and blue respectively; for each direction, a lighter shade is used for both orientations in the “+” sense and darker for both in the “-” sense.] They are tagged by a provisional label based on the orientations shown in this figure, and by their space group (a) “ ZY ” with $2 \times 2 \times 1$ cell, Orthorhombic $Pca2$ [here in the setting $P2ab$]. The bcc lattice corner clusters have the four directions $\pm Z_{r/l}$ while body-center clusters have the four directions $\pm Y_{r/l}$. (b) “ Z_2 ” with $2 \times 2 \times 1$ cell, Monoclinic $C2/c$; the $2 \times 2 \times 2$ supercell shown is two unit cells. Tetrahedra have two orientations, $\pm Z_r$. (c) “ XYZ ” with $4 \times 2 \times 2$ cell, CHECK space group in the setting ... The structure is shown as two slabs, each one lattice constant thick.

We saw three patterns in the whole range of pressures (actually strains):

- (1) at strain -0.020 , i.e. roughly $P < -2.3\text{GPa}$, we saw a structure we call “ ZY ” with a $2 \times 2 \times 1$ unit, thus 8 clusters per cell, which appears to have orthorhombic space group $Pca2$ [Figure 7(a)]

- (2) for strains -0.018 to -0.004 , i.e. pressures -2.3 to -0.6GPa , we found a simpler structure we call Z_2 containing just two cluster orientations which simply form (110) layers. [Figure 7(b)]. The space group is centered monoclinic $C2/c$ with 4 clusters per cell (=2 per primitive cell).

- (3) For strains -0.020 through 0.008 , i.e. up to a pressure of $\sim 1.4\text{GPa}$, we see the complex $4 \times 4 \times 2$ pattern shown in [Figure 7(c)], which has a triclinic (pseudo monoclinic) unit cell; there is a centering operation within the $4 \times 4 \times 2$ cell so there are 32 clusters per cell.

Finally, for the large strain of 0.010 (around $P = 1.6\text{GPa}$), we found a less regular $4 \times 4 \times 2$; we do not know if this is the true ground state.

We will describe the $4 \times 3 \times 2$ ordering pattern as a stacking of 4×4 layers along the z direction. The structure repeats after four of these layers (i.e. after two lattice constants, as there are layers of cell corners alternating with layers of body-center sites). We will use “flavor” to designate the X , Y , or Z nature of the orientation, so that each flavor includes four orientations. The even layers (cell corners) are of one kind that we call “ XY ” layers, after the orientation flavors found in them. The odd layers (body centers) are of another kind we will call “ XZ ” layers.

The basic ingredient of a layer is a chain with a pattern of orientations $AA\bar{A}\bar{A}$ where \bar{A} stands for inversion of A , where $A = X, Y$, or Z . Every layer is made by stacking such four chains side-by-side, using two alternating flavors; the second occurrence of the same flavor uses the orientations not found in the first one. In the XZ layers, the chains run in the x direction and are stacked in the y direction. Note that, if we draw bonds between neighbors of identical orientations, this forms a columnar pattern of dimers covering the square lattice. The XY layers have chains the other way around, running in the y direction and stacked in the x direction, but slightly different from the way in the XZ layers. The slight difference is that here, if we mark the adjacent pairs of the same orientation, it forms a *staggered* dimer pattern.

If we go up two layers, i.e. one lattice constant in the z direction, we get the same pattern, except all orientations are replaced by the complementary ones of the same flavor. Also, the registry between successive layers is such that (in projection) the X dimers in the XZ layer cross the Y dimers in the XY layer.

We also did simulations with smaller dimensions of supercell. Runs with a $2 \times 2 \times 1$ cell indeed give the same ground state as the $4 \times 4 \times 4$ whenever that state fits into the smaller supercell, i.e. for negative strains; for positive strains, the $2 \times 2 \times 1$ gives higher energy states, showing that the ground state cannot fit into that cell. (Monte Carlo results from a $3 \times 3 \times 3$ system are always higher in energy, presumably because the true ground state can never fit into an odd dimensioned cell.) Finally, we also exhaustively enumerated all 12^8 orientation combinations in the $2 \times 2 \times 1$ supercell. The ground states found in this way agree with the MC results whenever that shows a ground state with a $2 \times 2 \times 1$

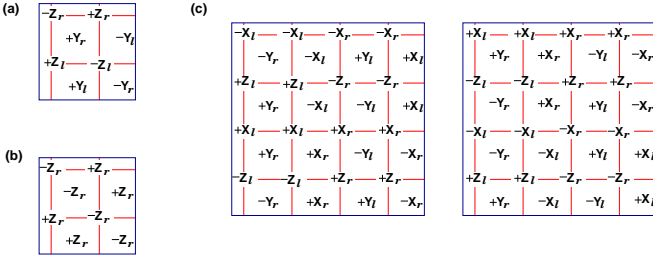


FIG. 8: The same structures shown in Figure 7, expressed in terms of the orientation labels defined in Sec. II A 1

supercell, i.e. at strains less than or equal to zero.

Brommer performed an exhaustive enumeration using a $\sqrt{2} \times \sqrt{2} \times 2$ supercell, (this contains 8 clusters). His best structure (see Ref. 19, Figure 4.13) appears to be our a phase, containing the four orientations $\pm Z_{r/l}$, which is similar but not identical to our result at zero pressure, which was the “ Z_2 ” phase. That is surprising, in view of the close similarity of our fitted potential to that of Brommer *et al* (see Sec.A, above).

2. Comparison with experiments

Our results are reminiscent of, but not in agreement with, the experiments, which find ordered states with unit cells of either $2 \times 2 \times 1$ or $2 \times 2 \times 2$. The experimental pressure-temperature (P - T) phase diagram of Watanuki *et al.*⁴ is shown in Figure 9. The ground state structure shown in Figure 7(b) agrees with the $C2/c$ proposed arrangement in Ref. 22 similar to one in Ref. 4

Direct comparison to experimental data is not possible since the $P > 0$ experiment is for a different alloy Cd_6Yb . Still, some similarities exist. Most importantly, the Z_2 phase, which we predict to be stable in the pressure range bracketing $P = 0$, is (apart from small rotations around z) the same $C2/c$ structure proposed in Figure 5 of Ref. 30 for the (ambient pressure) phase of $CaCd_6$. The $\{110\}$ structure suggested in Figure 3(c) of Ref. 4, for the low- and high-pressure phases of Cd_6Yb , is also the same as our Z_2 or Z_4 phase if we use zero rotations in place of the small right/left rotations.

We have not studied our model system at the highest pressures, so we do not know whether it has a counterpart for the highest-pressure phase of Ref. 4.

Watanuki *et al.*⁴ suggest that the reason that different phases are selected with increasing pressure is the competition of nearest-neighbor and longer-range interatomic interactions. The latter were due, they conjectured, to Friedel oscillations. (We point out that elastically mediated interactions are just as long-ranged as the oscillating part of the interatomic potential, both of these being ideally $1/R^3$.) However, we obtained a similarly complex phase diagram without refitting the EAM potentials (meaning that any change in Friedel oscillations was not explicitly taken into account). Within our approach, the reason for the multiple phases is that the orientational interaction of neighboring clusters is quite frustrated:

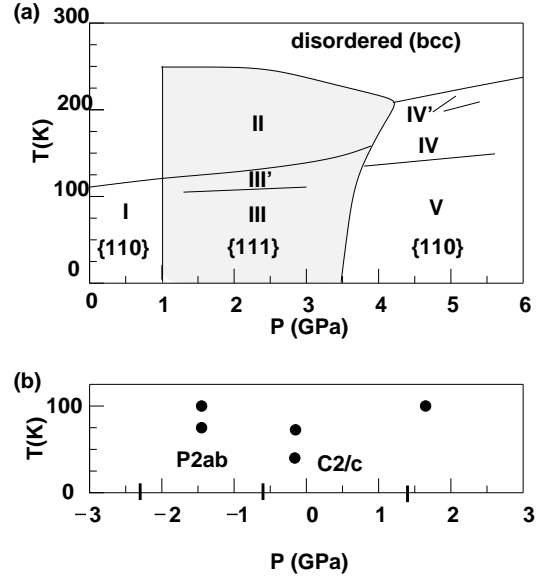


FIG. 9: (a) Pressure-temperature phase diagram of Cd_6Yb [after Watanuki *et al.*⁴, Figure 3(a)]. The ordering wavevector of each phase is indicated (higher temperature phases have similar order but partially disordered); region with $\{111\}$ phases is shaded. All transitions to the disordered (bcc) phase are continuous. (b) Our prediction for $CaCd_6$; note shift in the pressure axes. Critical pressures at $T = 0$ are indicated by vertical bars; critical temperatures with first-order transitions, as reported in Table IX for the three strains where this was measured, are shown by black circles.

low-energy ordering patterns cannot simultaneously satisfy all interactions. It seems there are several inequivalent ways to balance good interactions with bad interactions that are nearly degenerate. Thus, a small change in the relative cost of different orientation combinations is expected to tip the balance to a different pattern.³⁸

C. Transitions at $T > 0$

Tamura *et al.*³² found an order-disorder transition in $CaCd_6$ at $T \approx 100K$. Under pressure, in the similar system Cd_6Yb , Watanuki *et al.*⁴ found order-disorder transitions of the high-pressure phases too; order set in at $T = 200 - 250 K$, and a further ordering within that phase occurred at $T \approx 140 K$.

Simulations by Brommer *et al* based on their version of the discrete cluster pair Hamiltonian, using a $4 \times 4 \times 4$ simulation cell, found a first-order transition at $T \approx 91K$. Brommer pointed out¹⁹ this represents an entropy jump of about $1.0 k_B$ per cluster – twice what was estimated by Tamura *et al.*³³ for the similar compound Cd_6Y – and an energy jump of $\sim 10meV$ /cluster.

At present we only have preliminary data concerning transitions as a function of temperature. The tempering MC simulation, which requires running multiple replicas of the system at different temperatures, naturally detects discontinuities

strain	P (GPa)	T_c (K)	ΔE (meV/cluster)	ΔS (k_B /cluster)
-0.010	-1.46	72.5	3.359	0.537
		97.5	6.953	0.827
0.000	-0.14	40.0	0.547	0.159
		70.0	3.672	0.609
+0.010	1.65	100.0	6.641	0.770

TABLE IX: Thermal transitions at three fixed strains, along with the corresponding pressure at $T = 0$. The T_c is uncertain by ± 2.5 K. The jump in total energy is shown for each transition, divided by the number of clusters, and the corresponding entropy change ΔS per cluster is inferred (in units of Boltzmann’s constant).

in the energy as a function of temperature; our present results, shown in Table IX, are based purely on this metric. We took data from zero to high temperatures for three different choices of the strain: strongly negative, zero, and strongly positive, finding *two* first order transitions for the first two cases, but only one in the case of positive strains. Around zero strain, there seems to be a particular tendency to have closely competing states and low-energy excitations, and we believe this explains the one rather low transition temperature for that case.

Simulations by Brommer *et al*¹⁶ furthermore found a thermal ordering transition in a $4 \times 4 \times 4$ supercell; they did not analyze the orientation pattern in the ordered state there, but found its energy at the transition was only 1 meV/cluster higher than the $\sqrt{2} \times \sqrt{2} \times 1$ structure.

Presumably, both in experiment and in our simulations, the high- T phases are partially disordered versions of the low- T phases seen at the same pressure. In particular, the orientations related by a change of r to l suffix in their symbols differ by a comparatively small rotation, so possibly (see Sec. III A 1) they have similar interactions. Thus one possibility is that a partially disordered states has a sublattice containing (say) random, equal populations of $+X_r$ and $+X_l$ orientations.

In many ternary cases, also in ScZn_6 , the ordering transition is not sharp in experiments, which Tamura speculated indicates a glassy freezing. This is plausible in view of the frustrated orientational interactions we found.

VI. DISCUSSION

We will first summarize this work and then the outlook for extensions of it.

1. Summary

In this paper, we presented a comprehensive template for studying cluster interactions in CaCd_6 and more generally in any material possessing cluster orientation degrees of freedom. We showed how to operationally relate cluster orientations to atom positions (Sec. II C), worked out some group theory for the symmetry of the interactions (Sections II D 2

and III A), and fixed the technical obstacle of redundant parameters due to constraints in the pair counts (Sec. II D 3). Most of all, we showed that a singular value decomposition can clarify the dominant nature of the interaction and allows a long list of fitting parameters to be truncated to a manageable number (Sections II E and III A 2).

When this was actually applied to CaCd_6 , we found (in Sec. III B that the omitted interactions – of whatever form, multi-cluster or pair interactions with farther neighbors – amounted to only 1/100-1/10 of the nearest-neighbor pair interactions. The same is true even for pair interaction contributions apart from the first two singular vectors. This means that truncating to those two dominant terms, as about as realistic as the nearest-neighbor Heisenberg spin exchange, typically is, when used to model a magnetic material.

With effective interactions in hand, we carried out Monte Carlo simulations of larger lattices, for the purpose of discovering the optimum arrangements (Section V). This is difficult, as the interactions are frustrated leading to glassiness. Along with this, we made a rather sketchy study of the phase diagram, varying pressure and temperature. Its overall nature is broadly reminiscent of experiment (on CaCd_6 or isostructural compounds such as Cd_6Yb), in that several ordering patterns are encountered as pressure is varied, and there are also multiple transitions with increasing temperature, which we respect represent partial orderings.

Using our method of orientation-constrained relaxation (Sec. II C 2), it was possible to extend our analysis to *continuously* varying orientations of the clusters. For that case, augment couple the singular-value-decomposition with a decomposition in terms of rotational harmonics. We have not fully developed all that could be done with continuous orientations. One byproduct of this calculation, which was not available otherwise, is the *single-cluster* orientational potential energy. If the continuous type interactions can be parametrized usefully for Monte Carlo simulations, one application would be to study the *dynamics* of clusters including the paths by which they pass from one discrete well to another. (Such a study was done for ScZn_6 using all-atom molecular dynamics with pair potentials¹².)

2. Possible future work

One obvious direction for future work is to study the composition dependence. For example, diffraction found somewhat different ordering patterns as one varies the large atom component in isostructural alloys (Ca, Yb, and the other rare earths have slightly different sizes): e.g. $\sqrt{2} \times \sqrt{2} \times 2$ cell in 1/1- Cd_6Yb , a versus $\sqrt{2} \times \sqrt{2} \times 1$ C-centered monoclinic cell in 1/1- Cd_6Ga . Similarly, different critical temperatures were measured experimentally. Certainly, the strength of tetrahedron interactions will depend sensitively on the composition. In ScZn_6 ¹² the interactions are much weaker than in CaCd_6 but an ordering occurs nevertheless¹⁰.

Another direction is to thoroughly study the thermal behavior, which will require metrics to identify the nature of partially ordered states. This can also be extended to “approx-

mant” phases with larger cells such as the $2/1$ approximant of i -CdYb, which has four equivalent clusters per cubic cell; this shows a transition to tetrahedron orientational order, a complex stacking along a (100) direction³¹.

Our ultimate goal is to understand the tetrahedron orientations in the *quasicrystal* phase, and their role in stabilizing it. A speculative possibility is the implementation of matching rules by such clusters. Matching rules in the Penrose tiling (or its 3D analog) are markings that spoil the symmetry of otherwise rhombic or pentagonal objects, and enforce a deterministic, quasi-periodic arrangement analogous to an ideal crystal, thus offering one scenario for the stabilization of quasicrystals. It should be noted that the atomic structures of various icosahedral quasicrystals, understood as packings of fully symmetric clusters, showed no features that could implement such matching rules. Furthermore, there is a more economical alternative scenario that long-range order is emergent in dimension 3 from a “random tiling” in which the cluster packings sample an ensemble of extensive entropy. The random-tiling scenario found support (in various icosahedral quasicrystals, including i -CaCd) in the shapes of diffuse tails around Bragg peaks in diffraction experiments. Otherwise no decisive experiments are known, so the best approach to discover matching rules, if they exist, appears to be multi-scale simulation of the sort carried out in the present paper. The most plausible specific physical mechanism for matching rules in an icosahedral quasicrystal is via asymmetric inner clusters such as the tetrahedron in i -CaCd. These might be investigated in the future by extending the methods of this study to larger approximants such as $\text{Ca}_{13}\text{Cd}_{76}$ ²¹.

Acknowledgments

This work was supported by DOE Grant DE-FG02-89ER-45405 (WC, CLH, MM), and Slovak Research and Development Agency funding under contracts VEGA 2/0111/11 and APVV-0076-11 (MM). We are grateful to P. Brommer for providing the interaction matrices computed in Refs. 16 and 19.

Appendix A: Comparison to Brommer *et al* fit

We were provided the interaction matrices computed by Brommer *et al*¹⁶. They had recognized the redundancies in the fit, and resolved them arbitrarily by setting certain terms to zero. That meant the magnitude of any particular pair interaction $V_{\alpha\beta}$ could not be given a physical interpretation: such interactions are valid only for computing the total energy of an entire configuration. However, if one applies our recipe to resolve redundancies from Sec. IID 3 to their $V_{\alpha\beta}$, we get a well-defined result which can be compared with ours.

We expect a great similarity to our EAM results, since we

used the same potentials as they did. The important differences in our calculation are

- (a) For a database, out of the approaches we described in Sec. IID 1, they used random whole configurations whereas we used the uniform background.

σ	irrep	$+X_r$	$-X_l$	$+X_l$	$-X_r$
27.69	E	0.5542	0.5542	0.1617	0.1617
		3.9	-3.9	-160.6	160.6
32.62	E	0.3927	0.3927	0.4232	0.4232
		-91.2	91.2	125.8	-125.8
22.6	E	0.4139	0.4139	0.4025	0.4025
		-104.3	104.3	-148.9	148.9
18.25	I	0.3401	-0.3401	-0.2259	0.2259
13.15	I	0.2887	0.2887	-0.2887	-0.2887
7.385	E	0.1842	0.1842	0.5472	0.5472
		44.8	-44.8	48.8	-48.8
5.404	I	0.2259	-0.2259	0.3401	-0.3401

TABLE X: Results from Brommer *et al*, Ref. 16: singular values and right singular vectors for c -linkage, same format as table III. Note the symmetries relating the pair of columns for $+X_r$ and $-X_r$, and similarly relating the columns for $+X_l$ and $-X_l$: they have the same magnitudes and, for representation E , they have opposite phase angles (after removal of an overall arbitrary phase).

- (b) They did not use constrained relaxation, but relied on the final states corresponding to the initial ones. (See our discussion in Sec. IIC 2.) Furthermore, their initial state was not one of the twelve idealized orientations inferred from relaxations, but one of the Gomez-Lidin orientations, postulated on the basis of diffraction.

The results look similar for the b -linkage interaction matrix. When we perform the SVD analysis, the overall pattern of singular values seen in Table XI is similar to what we saw in Table IV), though with slightly less of a separation between large and small singular values. However, the dominant singular vector comes from a different representation, and the pattern of signs in the singular vectors is also different. (It is likely these differences are artifacts of different conventions we used for the orientations; Ref.¹⁶ used the other choice for orienting icosahedral axes in cubic symmetry, differing from ours by a 90° rotation.

On the other hand, the results for the c -linkage interaction matrix look completely different, as does the singular value decomposition (Table X). Furthermore, for reasons we do not understand, the latter exhibits an additional symmetry relating the columns differing by the sense $+$ and $-$ of the orientation, which does not correspond to *any* symmetry of the clusters. Finally, the c -linkage singular values are large and (unlike all other cases analyzed in this paper) the magnitudes of the largest and smallest ones do not differ by a large factor.

* Electronic address: wc274@cornell.edu

† Electronic address: clh@ccmr.cornell.edu

σ (meV)	irrep	$+X_r$	$+Y_r$	$+Z_r$	$-Z_l$
69.37	B_2	-0.1587	-0.4741	0	0
21.75	A_1	-0.0851	0.1515	0.3978	-0.5305
6.194	A_1	0.0064	0.3327	-0.4950	-0.1832
5.415	B_2	-0.4741	0.1587	0	0
4.787	B_1	0.4921	0.0885	0	0
4.280	A_2	0.1681	0.1638	0.4602	-0.4220
2.415	A_2	0.0087	-0.4041	0.3967	0.1259
1.672	A_2	0.1684	-0.2417	-0.3588	-0.4446
8.392×10^{-1}	B_1	0.0885	-0.4921	0	0
7.456×10^{-1}	A_2	-0.4396	-0.0380	0.0464	-0.3292
7.442×10^{-2}	A_1	0.3992	-0.1818	-0.1160	-0.3189

TABLE XI: Results from Brommer *et al*, Ref. 16: singular values and right singular vectors for b -linkage, same format as table IV.

- ¹ A.P. Tsai, J. Q. Guo, E. Abe, H. Takakura, and T. J. Sato, Nature 408, 537-8 (2000).
- ² H. Takakura, J. Q. Guo, and A.-P. Tsai, Phil. Mag. Lett. 81, 411 (2001).
- ³ J. Q. Guo, E. Abe, and A. P. Tsai, Phys Rev. B 62, R14605 (2000).
- ⁴ T. Watanuki, A. Machida, T. Ikeda, K. Aoki, H. Kaneko, T. Shobu, T. J. Sato, and A. P. Tsai, Phys. Rev. Lett. **96**, 105702 (2006).
- ⁵ R. Tamura, "Properties of Cd-Based Binary Quasicrystals and Their 1/1 Approximants" Isr. J. Chem. 51 SI 1263-1274 (2011).
- ⁶ M. Mihalkovič and C. L. Henley, preprint arXiv:1112.3804.
- ⁷ K. Nozawa and Y. Ishii, J. Phys. Condens. Mat. 20, 315206 (2008).
- ⁸ "Experimental evidence for a phase transition in a Zn_6Sc 1/1 cubic approximant" T. Yamada, R. Tamura, Y. Muro, et al. Phys. Rev. B 82, 134121 (2010).
- ⁹ K. Nishimoto, R. Tamura, and S. Takeuchi, Phys. Rev. B 81, 184201 (2010). Phys. Rev. B 81, 184201 (2010) [5 pp] "In situ transmission electron microscopy observation of an orientational order-disorder transition in Cd_6Eu and Cd_6Ce crystalline approximants",
- ¹⁰ H. Euchner, T. Yamada, H. Schober, S. Rols, M. Mihalkovič, R. Tamura, T. Ishimasa, and M. de Boissieu, J. Phys. Condens. Matter 24, 415403 (2012), "Ordering and dynamics of the central tetrahedron in the 1/1 Zn_6Sc periodic approximant to quasicrystal"
- ¹¹ T. Hatakeyama, K. Nozawa and Y. Ishii, Z. Kristallogr. 223, 830-832 (2008)
- ¹² M. Mihalkovič and C. L. Henley, Philos. Mag. xx, 1 (2011).
- ¹³ C. P. Gómez and S. Lidin, Phys. Rev. B. **68**, 024203 (2003).
- ¹⁴ A. Palenzona, J. Less-Common Met. 25, 367 (1971).
- ¹⁵ P. Brommer and F. Gähler, Philos. Mag. 86, 753-758 (2006).
- ¹⁶ P. Brommer, F. Gähler, and M. Mihalkovič, Philos. Mag. **87**, 2671 (2007). P. Brommer, F. Gähler, and M. Mihalkovič, Philos. Mag. **87**, 2671-2677 (2007).
- ¹⁷ Marek Mihalkovič and C. L. Henley, Phys. Rev. B 85, 092102 (2012).
- ¹⁸ S-Y Piao, C. P. Gomez, and S. Lidin, Z. Naturforsch. 60b, 644-9 (2006.)

- ¹⁹ P. Brommer, Ph. D. thesis (Universität Stuttgart, 2008): "Development and Test of Interaction Potentials for Complex Metallic Alloys"
- ²⁰ E. R. Grannan, M. Randeria, and J. P. Sethna, Phys. Rev. Lett. 60, 1402 (1988).
- ²¹ C. P. Gomez, Angew. Chemie 40, 4037 (2001).
- ²² R. Tamura, K. Nishimoto, S. Takeuchi, K. Edagawa, M. Isobe, and Y. Ueda, Phys. Rev. B **71**, 092203 (2005).
- ²³ J. R. Shewchuk, "An Introduction to the Conjugate Gradient Method Without the Agonizing Pain", online resource <http://www.cs.cmu.edu/~quake-papers/painless-conjugate-gradient.pdf>, page 52.
- ²⁴ C. L. Henley, Phys. Rev. B43, 993 (1991).
- ²⁵ J. Richmond-Decker, B.S. thesis (Cornell University, 2012); J. Richmond-Decker, D. Chaudhuri, M. Mihalkovič, and C. L. Henley, unpublished.
- ²⁶ Uzi Hizi, Ph. D. thesis, Cornell University (2006).
- ²⁷ M. Mihalkovič, J. Richmond-Decker, C. L. Henley, and M. Oxborrow, "Ab-initio tiling and atomic structure for decagonal $ZnMgDy$ quasicrystal" (preprint 2011) arXiv:1112.3951
- ²⁸ J. K. Mason and C. A. Schuh, Acta Materialia 56, 6141 (2008).
- ²⁹ J. Z. Jiang, L. Gerward, and J. S. Olsen, Appl. Phys. Lett. 79, 2538 (2001).
- ³⁰ R. Tamura, K. Edagawa, K. Shibata, K. Nishimoto, S. Takeuchi, K. Saitoh, M. Isobe, and Y. Ueda, Phys. Rev. B 72, 174211 (2005).
- ³¹ R. Tamura, K. Minoda, S. Takeuchi, K. Edagawa, T. Kiss, T. Yokoya, and S. Shin, Philos. Mag. 86, 489-497 (2006).
- ³² R. Tamura, Y. Murao, S. Takeuchi, M. Ichihara, M. Isobe and Y. Ueda, Jap. J. Appl. Phys. 40, L912 (2002).
- ³³ R. Tamura, K. Edagawa, C. Aoki, S. Takeuchi, and K. Suzuki, Phys. Rev. B, 68, 174105 (2003).
- ³⁴ Our definition is intended strictly for $T = 0$. At finite temperature, the effective Hamiltonian should properly be defined as a free energy, including both energy and entropy contributions, and sampling all configurations with the given tetrahedron orientations. That would obviously be much harder to evaluate from simulations.
- ³⁵ The "classical" potentials are of course by anchored fitting to electronic calculations that are based, via the Local Density Approximation, to the many-electron Schrödinger equation. They are classical in the sense that they are deterministic functions of the atomic positions, having integrated out the electron wavefunctions and neglected the ionic zero-point motions.
- ³⁶ Actually, our resolution of the redundancy is equivalent to projecting away the subspace in $V_{\alpha\beta}$ parallel to $(1, 1, 1, \dots)$ so its rank was reduced by one. Therefore, the last singular value σ_m is always zero.
- ³⁷ Interestingly, Figure 3 demonstrates that any uniform background state is about 20 meV/cluster higher in energy than a typical random pattern.
- ³⁸ A change in the relative strength of $\langle 1/2, 1/2, 1/2 \rangle$ versus $\langle 1, 0, 0 \rangle$ type cluster pair interactions could be part of this change. This might be similar in its mechanism to the change posited in Ref. 4, but is not the same, since they imagined a change in the ratio of hard-core and long-range interactions.